Palaeogeography, Palaeoclimatology, Palaeoecology 594 (2022) 110961

Contents lists available at ScienceDirect

Palaeogeography, Palaeoclimatology, Palaeoecology

journal homepage: www.elsevier.com/locate/palaeo

Multi-proxy investigation of the post-evaporitic succession of the Piedmont Basin (Pollenzo section, NW Italy): A new piece in the Stage 3 puzzle of the Messinian Salinity Crisis

F. Andreetto [a,*], A.M. Mancini [b], R. Flecker [c], R. Gennari [b], J. Lewis [d], F. Lozar [b], M. Natalicchio [b], F. Sangiorgi [a], M. Stoica [e], F. Dela Pierre [b], W. Krijgsman [a]

[a] Department of Earth Sciences, Utrecht University, Budapestlaan 17, Utrecht 3584, CD, the Netherlands
[b] Dipartimento di Scienze della Terra, Università di Torino, Via Valperga Caluso 35, 10125 Torino, Italy
[c] BRIDGE, School of Geographical Sciences and Cabot Institute, University of Bristol, University Road, Bristol BS8 1SS, UK
[d] Bristol Isotope Group, School of Earth Sciences, University of Bristol, Wills Memorial Building, Queen's Road, Bristol BS8 1RJ, UK
[e] Department of Geology, University of Bucharest, Bălcescu Bd. 1, Bucharest 010041, Romania

ARTICLE INFO

Editor: Dr. A Dickson

Keywords:
Lago-Mare
Piedmont Basin
Mediterranean connectivity
Strontium isotopes
Messinian Salinity Crisis

ABSTRACT

Paleoenvironmental reconstruction of the Mediterranean Basin at the end of the Messinian Salinity Crisis is contentious. One section that records this final phase (Stage 3) is the Pollenzo Section in the Piedmont Basin (NW Italy). Here, we present new stratigraphic, sedimentological, petrographic, micropaleontological (ostracods, calcareous nannofossils, foraminifera, dinoflagellates) and geochemical ($^{87}Sr/^{86}Sr$ ratios) data from the Cassano Spinola Conglomerates (CSC) and interpret the paleoenvironment of this northernmost tip of the Mediterranean Basin. The CSC comprise three depositional units: members A and C, which were deposited subaqueously, and the intervening member B, which is continental. The CSC is topped by a ~ 50 cm-thick black layer, which is directly overlain by the open marine Argille Azzurre Formation of early Zanclean age. Our investigation reveals that member A is largely barren of autochtonous microfossils, except for an almost monospecific ostracod assemblage of *Cyprideis torosa* at the top, which indicates shallow-water (<30 m) conditions. Paratethyan ostracods and, possibly, taxa of calcareous nannofossils adapted to low-salinity water first occur in member C. $^{87}Sr/^{86}Sr$ ratios measured on ostracod valves from the member A/B transition (0.708871–0.708870) and member C (0.708834–0.708746) are lower than the coeval Messinian seawater values (~0.709024) and the $^{87}Sr/^{86}Sr$ ratios of a hypothetical lake filling Piedmont (>0.7090) estimated by means of the present-day $^{87}Sr/^{86}Sr$ signature of the Po river, the main drainage system of Northern Italy that receives the weathering products (including ions) of the Alps and Apennines. These values are likely to reflect the mixing of local high $^{87}Sr/^{86}Sr$ river water with low $^{87}Sr/^{86}Sr$ from the Mediterranean, which at the time was dominated by inputs from Eastern Paratethys, circum-Mediterranean rivers and Atlantic Ocean. Our results suggest that, at times during the final stage of the Messinian Salinity Crisis, the Piedmont Basin was hydrologically connected with the main Mediterranean Basin. At regional scale, this implies that the water level in the Mediterranean Basin was relatively high.

1. Introduction

The terminal Stage 3 (5.55–5.332 Ma) of the Messinian Salinity Crisis (MSC) in the Mediterranean (5.97–5.332 Ma; Roveri et al., 2014a) has attracted attention over the last two decades as attempts are made to integrate a variety of different data of this interval (Roveri et al., 2008a; Andreetto et al., 2021a). The nub of the controversy concerns the isolation or connectivity between the Stage 3 depocentres. One end-member hypothesis argues that Stage 3 sedimentation happened in endorheic lakes (e.g. Hsü et al., 1973, 1978; Cita et al., 1978, 1990; Orszag-Sperber et al., 2000; Ryan, 2009; Madof et al., 2019, 2022; Caruso et al., 2020; Heida et al., 2021; Raad et al., 2021). The other suggests that water sources such as Atlantic and/or Eastern Paratethys and large Mediterranean rivers (e.g. Nile and Rhône) filled the

* Corresponding author.
E-mail address: f.andreetto@uu.nl (F. Andreetto).

https://doi.org/10.1016/j.palaeo.2022.110961
Received 19 October 2021; Received in revised form 21 March 2022; Accepted 24 March 2022
Available online 29 March 2022

Mediterranean sufficiently to link more marginal and deeper subbasins together (McCulloch and De Deckker, 1989; Roveri et al., 2008a, 2014b, 2014c; Manzi et al., 2009, 2016; Marzocchi et al., 2016; Stoica et al., 2016; Gvirtzman et al., 2017; Pellen et al., 2017; Vasiliev et al., 2017; García-Veigas et al., 2018), at least episodically (Andreetto et al., 2021b). Much of this controversy originates from the interpretation of the Stage 3 fossil records, which yield both marine and brackish, Paratethys-derived fossils (Benson, 1978; Cita et al., 1978; Iaccarino and Bossio, 1999; Roveri et al., 2008a; Guerra-Merchán et al., 2010; Cosentino et al., 2012; Popescu et al., 2015, 2021; Pellen et al., 2017; Andreetto et al., 2021a for further references). Associations mixing fossils with different ecological requirements always pose a challenge to the reconstruction of the paleodepositional environment(s), because it is often unclear which are reworked and which coeval with sedimentation (e.g. Bright et al., 2018).

The sub-basins at the periphery of the Mediterranean system are a good location for testing the isolated/connected hypothesis, since evidence of connectivity with the Atlantic and/or Eastern Paratethys requires the Mediterranean Basin to have been relatively full. The Piedmont Basin at the northernmost tip of the Mediterranean system, which was, during the late Messinian, enclosed on three sides by the Alps and the Apennines and open to the Mediterranean to the east via the Po Plain foredeep and Adriatic Basin (Fig. 1a; Boccaletti et al., 1990; Foeken et al., 2003; Beltrando et al., 2010; Cosentino et al., 2018), meets

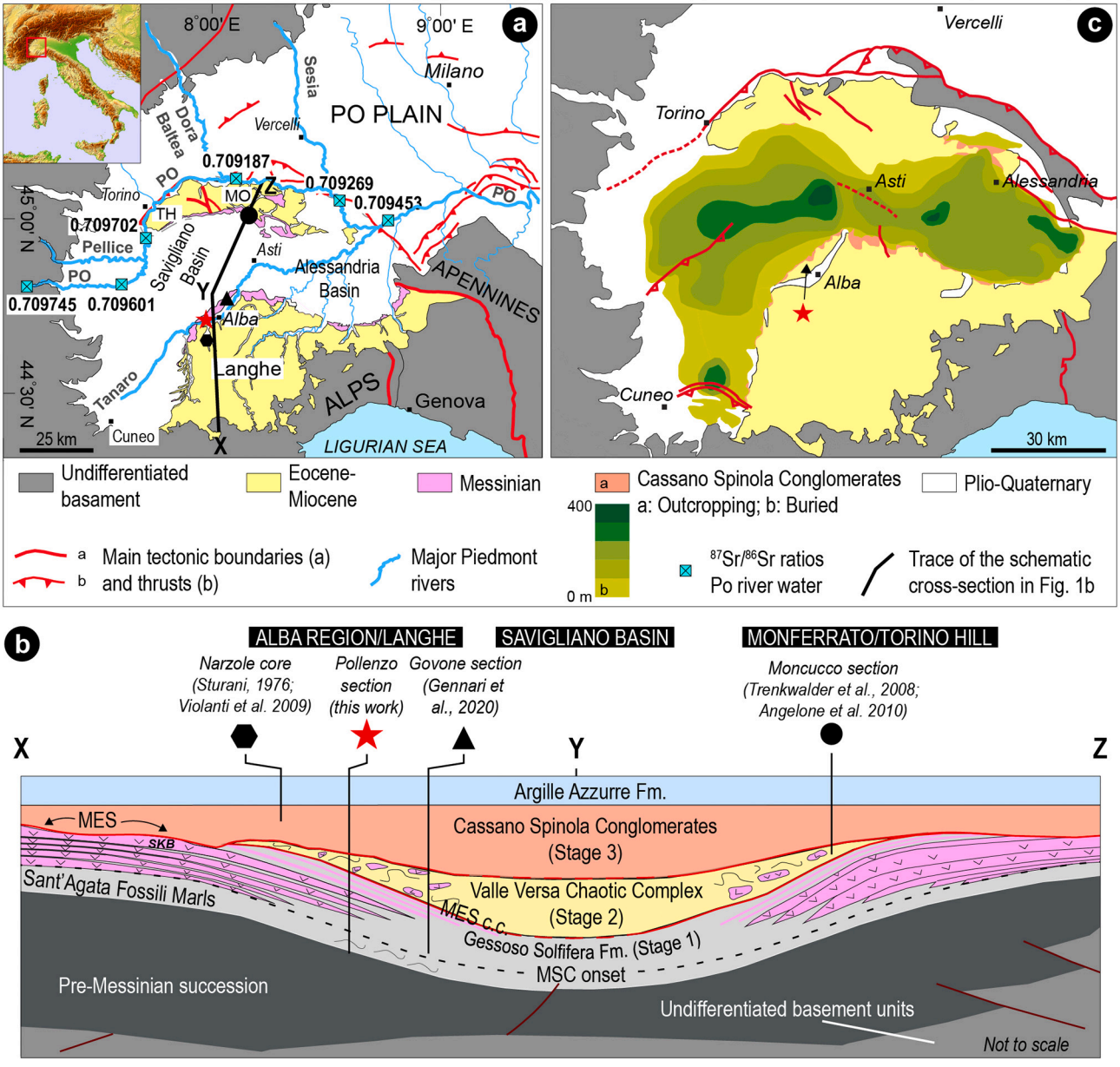

Fig. 1. a. Structural sketch map of the Piedmont Basin showing the location of the studied Pollenzo section (red star) and of other sites studied for their Stage 3 sedimentary record (black hexagon: Narzole core; black triangle: Moncucco section) or mentioned in the text (Govone section; black circle). The $^{87}Sr/^{86}Sr$ ratios of the Po river water (from Marchina et al., 2018) employed to constrain the $^{87}Sr/^{86}Sr$ signature of a hypothetical Piedmont lake (see paragraph 6.2 for insights) is also shown. TH: Torino Hill; MO: Monferrato. **b.** Schematic cross-section through the Piedmont Basin emphasizing the latero-vertical relationships between the MSC and pre-MSC lithostratigraphic units (modified from Dela Pierre et al., 2011). The trace of the cross section is reported in Fig. 1a. SKB: Sturani key-bed; MES: Messinian erosional surface; MES c.c.: correlative conformity of the Messinian erosional surface. **c.** Surface and subsurface distribution of the CSC in the Savigliano and Alessandria Basins (modified from Irace et al., 2009). (For interpretation of the references to color in this figure legend, the reader is referred to the web version of this article.)

these geographical criterion. The Cassano Spinola Conglomerates (CSC) assigned in the Piedmont Basin to Stage 3 (Dela Pierre et al., 2011) have, however, received far less attention than both pre-Stage 3 deposits in the same region (Irace et al., 2005; Dela Pierre et al., 2002, 2007, 2011, 2012, 2014, 2015; Lozar et al., 2010, 2018; Violanti et al., 2013; Natalicchio et al., 2014, 2017, 2019, 2021; Gennari et al., 2020; Pellegrino et al., 2020; Sabino et al., 2020, 2021; García-Veigas et al., 2021) and time-equivalent deposits exposed onland elsewhere in the Mediterranean (see Andreetto et al., 2021a). Existing studies of the CSC have largely focused on the paleontological study of the macrofossiliferous content (Sardella, 2008; Angelone et al., 2011; Colombero et al., 2013, 2014, 2017; Harzhauser et al., 2015; Grunert et al., 2016; Carnevale et al., 2018), whereas few papers have explored the micropaleontological content and geochemical signatures of its fine-grained subaqueous portions (Sturani, 1973; Trenkwalder et al., 2008; Esu and Popov, 2012), which might contain the evidence of the hydrological input from the Mediterranean Basin.

In this paper we present results from a continuous exposure of the CSC preserved in the Pollenzo section. These include lithological, sedimentological, micropaleontological (ostracods, foraminifera, calcareous nannofossils, dinoflagellates) and geochemical ($^{87}Sr/^{86}Sr$ ratios) analyzes. The results will be discussed in the context of evolving base level and hydrological changes simultaneously affecting the Mediterranean and impacting its connectivity with its northernmost branch.

2. Geological setting

The Piedmont Basin (NW Italy, Fig. 1a) is a wedge-top basin that developed on a tectonic wedge of Alpine, Ligurian and Adria basement units juxtaposed during the mesoalpine collisional event between the Adriatic promontory and the European plate (e.g. Schmid and Kissling, 2000; Carrapa and Garcia-Castellanos, 2005; Beltrando et al., 2010). Since the late Oligocene, the basin was involved in N-verging Apennine tectonics that finally resulted in overthrusting on the Padane foredeep along the Pliocene-Pleistocene Padane Thrust Front (e.g. Mosca et al., 2009; Rossi, 2017; Ghielmi et al., 2019). The Piedmont Basin comprises 4000–5000 m of upper Eocene-Holocene sediments. The upper Eocene-lower Oligocene units consist of continental and shallow marine sediments grading up into upper Oligocene-upper Miocene deeper water hemipelagites with interbedded turbiditic sandstones recording the main accretionary phases of the Apennine fold and thrust belt (Rossi, 2017). Gypsum bodies and hyposaline sediments bearing Paratethyan fossils were deposited during the MSC (Sturani, 1973; Dela Pierre et al., 2011; Ghielmi et al., 2019). MSC deposits reach a maximum thickness in the Savigliano (~500 m; Irace et al., 2009) and Alessandria sub-basins (~800 m; Irace et al., 2009), where they are buried underneath km-thick Plio-Quaternary deposits (Fig. 1a–b). Zanclean marine deposits seal the MSC succession (Trenkwalder et al., 2008; Violanti et al., 2009, 2011).

3. The Messinian of Piedmont

3.1. General stratigraphy and architecture

Following the stratigraphic scheme developed by Dela Pierre et al. (2011) along the south-western margin of the Piedmont Basin (Langhe in Fig. 1a), the Messinian succession comprises, from bottom to top, the following lithostratigraphic units (Fig. 1b): the Sant'Agata Fossili Marls (SAF) representing the pre-MSC interval and, in the deeper part of the Piedmont Basin, part of MSC Stage 1; the Primary Lower Gypsum Unit (PLG), Vena del Gesso Fm. or Gessoso Solfifera Fm., entirely deposited during MSC Stage 1; the Valle Versa Chaotic Complex (VVC), equivalent of the Resedimented Lower Gypsum Unit (RLG) of Roveri et al. (2014a) and deposited during MSC Stage 2; the Cassano Spinola Conglomerates (CSC) representing (at least part of) MSC Stage 3.

The Sant'Agata Fossili Marls (Tortonian-Messinian) consist of shelf to slope calcareous microfossil-bearing marls and organic-rich laminated shales arranged in 2–3 m-thick sedimentary cycles related to precession (Lozar et al., 2010, 2018; Dela Pierre et al., 2011; Violanti et al., 2013). At 5.97 Ma gypsum precipitation started at the basin margins, synchronously to other potentially silled basins around the Mediterranean margins (Krijgsman et al., 1999a, 1999b; Lugli et al., 2010; Manzi et al., 2013). The onset of gypsum deposition is progressively younger towards the depocenter of the Piedmont Basin, where gypsum layers are replaced by marls (Dela Pierre et al., 2011; Ghielmi et al., 2019; Gennari et al., 2020; Fig. 1b). Barren shales are interbedded with both the gypsum and the marl layers (Dela Pierre et al., 2011). The PLG unit in the Piedmont Basin has similar lithofacies and stratigraphic stacking pattern of coeval gypsum deposits described in other Mediterranean marginal localities (e.g. Sorbas and Nijar basins in SE Spain, Vena del Gesso Basin in the Northern Apennines and Zakynthos; Krijgsman et al., 1999a, 1999b; Lugli et al., 2010; Manzi et al., 2013; Karakitsios et al., 2017). In these settings, the lithologic cyclicity was ascribed to precession-driven climate changes and the sedimentary cycles tuned to the precession curve, with gypsum and marls reflecting drier climate at precession maxima (insolation minima) and the intervening shales recording more humid conditions at precession minima (insolation maxima; Krijgsman et al., 1999a, 1999b; Lugli et al., 2010; Roveri et al., 2014a). Given the aforementioned similarities, Dela Pierre et al. (2011) provided a similar interpretation of the PLG of the Piedmont Basin. More recently, fluctuations in major and trace elements, total organic carbon (TOC) and molecular fossils content in the marl-shale alternations of the Pollenzo (Natalicchio et al., 2019) and Govone (Sabino et al., 2020) sections revealed for the first time independent evidence that the lithological cyclicity of the Piedmont PLG was precession-driven, with the phase relations between the lithofacies and the orbital parameters hypothesized by Krijgsman et al. (1999a, 1999b).

The PLG is truncated at the top by an erosional surface progressively cutting into older beds towards the basin margins (Fig. 1b; Dela Pierre et al., 2011). This erosional surface is associated with an angular unconformity, particularly noticeable in seismic profiles (Ghielmi et al., 2019), suggesting uplift and deformation of the basin margin during the intra-Messinian tectonic phase (Dela Pierre et al., 2007). Dela Pierre et al. (2011) attributed this surface to the Messinian Erosional Surface (MES), traditionally ascribed to either a modest (<200 m; Roveri et al., 2014c) or extreme (several hundreds to thousands of meters; e.g. Clauzon, 1982; Loget et al., 2006; Amadori et al., 2018) base-level fall concomitant with the intra-Messinian tectonic phase (see Roveri et al., 2014a). Towards the basin depocenter, the MES passes into a correlative conformity flooring m-thick chaotic bodies emplaced by various types of gravity flows and including blocks of carbonates and MSC evaporites ranging in size from few meters to hundreds of meters (Dela Pierre et al., 2002, 2007, 2011). These sediments, both outcropping (VVC, Dela Pierre et al., 2002, 2007; Irace et al., 2005) and buried (Castellania Chaotic Complex of Ghielmi et al., 2019), are equivalent to the RLG unit that is found in several Mediterranean localities (e.g. Northern Apennines, Sicily, Cyprus; Roveri et al., 2001; Manzi et al., 2016, 2021). The VVC accumulated in various depocenters in the Piedmont Basin with variable thickness ranging from few meters up to 200 m (Ghielmi et al., 2019).

The VVC is capped by another erosional unconformity which merges with the MES at the basin margins (Fig. 1b; Dela Pierre et al., 2011). This surface is overlain by fine-grained deposits interbedded with sandstones and conglomerates. These sediments are currently grouped in the CSC, which reaches a maximum thickness of 100 m (Ghielmi et al., 2019). Lateral equivalent deposits of the CSC, now buried at depth in the Savigliano and Alessandria basins, have been observed in ENI seismic profiles and boreholes (https://www.videpi.com/videpi/pozzi/consultabili.asp). In the Savigliano Basin they are grouped in a single seismic sequence (ME3b) with maximum estimated thickness of ~370 m (Fig. 1c; Ghielmi et al., 2019). The stratigraphic architecture of the CSC and equivalent seismic unit(s) is, however, poorly known, as a

consequence of the scarcity of outcrops (Fig. 1c) and the absence of marker beds suitable for basin-wide physical stratigraphic correlations.

The Pollenzo section is the only locality in the Piedmont Basin where a continuous section from the Stage 2 VVC to the basal Zanclean open marine deposits (Argille Azzurre Formation, AAF) is exposed. The base of the AAF marks the end of the MSC and is dated at 5.332 Ma (Trenkwalder et al., 2008; Violanti et al., 2011) as elsewhere in the Mediterranean (Roveri et al., 2014a).

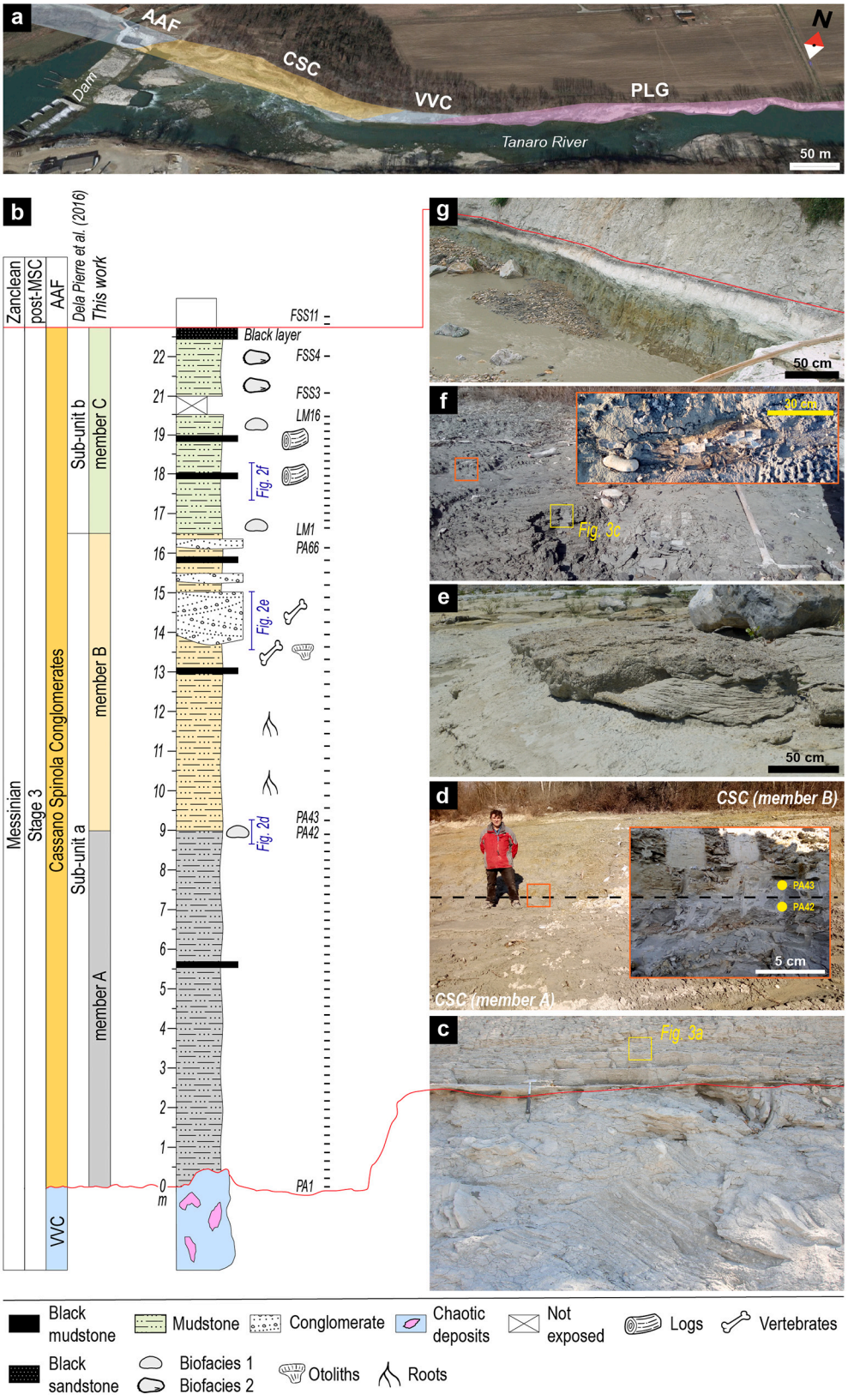

Fig. 2. **a.** Aerial view of the Pollenzo section (image credit: Google Earth) showing the distribution of the Messinian lithostratigraphic units. PLG: Primary Lower Gypsum; VVC: Valle Versa Chaotic Complex; CSC: Cassano Spinola Conglomerates; AAF: Argille Azzurre Fm. **b.** Detailed sedimentary log of the Cassano Spinola Conglomerates in the Pollenzo section. The exposure gap in member C is due to the recent construction of a dam (see Fig. 2a). **c-g.** Outcrop view of the Cassano Spinola Conglomerates: **c.** close up of the boundary between the VVC and the CSC. **d.** Member A/B boundary (dotted line). The inset shows a close up of the boundary, which corresponds to a marked change in color of the sediments from greyish (member A) to yellowish (member B). **e.** Outcrop view of the lowermost conglomerate layer. **f.** Member C, mostly composed of grey laminated mudstones. The inset shows a close view of a land plant remain, which corresponds to the bark of a tree trunk. **g.** The M/P boundary at the top of a prominent and laterally continuous black layer, which divides Paratethyan ostracod-rich mudstones of the CSC from open marine fauna-rich marls of the AAF. The different color of the member C mudstones is due to weathering. This picture is taken from Dela Pierre et al. (2016) and predates the building of the dam.

3.2. The Pollenzo section

The Pollenzo section (44°41′08″N, 7°55′33″E), located in the southern part of the Piedmont Basin in an intermediate position between the basin margin and the depocenter, records the entire Messinian succession (Figs. 1b, 2a). The section begins with the Sant'Agata Fossili Marls, which show a precession-driven cyclic stacking pattern given by couplets of laminated shales and marls (Lozar et al., 2010; Dela Pierre et al., 2011; Natalicchio et al., 2017). Indurated carbonate-rich beds are found intercalated with the marls in the upper part of the unit (Dela Pierre et al., 2012). In detail, seven lithological, precession-driven cycles were recognized in the topmost portion of this unit above a slump (Dela Pierre et al., 2011). The overlying PLG unit comprises 9 lithological cycles composed of shales and different types of gypsum lithofacies (massive selenite in the lower two cycles; laminar gypsum and branching selenite in the remaining cycles; Dela Pierre et al., 2011; Natalicchio et al., 2021). Physical stratigraphic, biostratigraphic and cyclostratigraphic data allowed the onset of the MSC to be identified three cycles below the base of the PLG (Lozar et al., 2010, 2018; Dela Pierre et al., 2011). The PLG is overlain by ~5 m of slumped mudstones enclosing up to meter-sized blocks of PLG gypsums and carbonates attributed to the VVC, the basal surface of which corresponds to the MES.

The section continues with the CSC (Fig. 2b). It was subdivided into two sub-units by Dela Pierre et al. (2016): sub-unit a, that comprises grey to yellowish mudstones, sandstones and conglomeratic lenses with terrestrial mammal and fish fossils (Colombero et al., 2013; Carnevale et al., 2018); sub-unit b, which largely consists of grey-green mudstones with a distinct mollusk assemblage comprising both species endemic to the Mediterranean and indigenous of the Eastern Paratethys (see Sturani, 1973, 1976 and Esu and Popov, 2012 for details on the mollusks). The top of the CSC and the boundary with the overlying AAF was submerged in 2014 by the building of a dam on the Tanaro River (Fig. 2a). Earlier studies of this interval describe the boundary as a dm-thick, black layer burrowed at the top (Sturani, 1973; Dela Pierre et al., 2016; Fig. 2b).

4. Material and methods

Field studies of the lithological and sedimentological characteristics of the CSC have been carried out at Pollenzo in February 2019 and a detailed stratigraphic section was logged (Fig. 2b). A total of 82 samples of mudstones were collected: 42 from member A (samples PA1–42), 24 from member B (samples PA43–66) and 16 from member C (samples LM1–16; see paragraph 5.1 for the definition of the members). Four additional samples from the stratigraphic interval now under water and collected previously by some of the authors (FD, FL, MN) have also been analyzed: two (FSS3–4) from the top of the CSC and two (FSS10–11) from the base of the Zanclean AAF, 30 and 35 cm above the Miocene/Pliocene (M/P) boundary. Samples were processed for sedimentological, petrographic (composition and mineralogy) and paleontological (ostracods, foraminifera, nannofossils and dinoflagellate cysts) observations using standard techniques. $^{87}Sr/^{86}Sr$ isotopes were analyzed on samples that contain Ca^{2+}-bearing minerals that satisfy three requirements: (1) they must not be reworked; (2) they must not have undergone significant diagenetic alteration with the introduction of exogenous Sr after formation; (3) in case fossil shells are selected: (3.1) they must be cleaned of the surrounding matrix, which is a contaminant; (3.2) they should be preferentially composed of low-Mg calcite, which is more resistant (i.e. less soluble) to post-depositional alteration than high-Mg calcite and aragonite skeletal grains (Bennett et al., 2011; Marcano et al., 2015). In light of the above, seven samples were selected for which sufficient ostracod (PA42–43, LM14–15, FSS3–4) and planktic foraminifera (FSS11) material was available. Analyzes were conducted at the Bristol isotope group Laboratory at Bristol University following the procedure outlined by Lewis et al. (2017).

A detailed description of the methods is provided as supplementary data (file S1).

5. Results

5.1. Field and petrographic observations

In the Pollenzo section, three members of the ~20 m-thick CSC can be recognized on the basis of lithological features.

Member A is a ~ 9 m-thick monotonous muddy succession resting on the erosional surface above the VVC (Fig. 2c). It is mainly composed of dark grey laminated silty mudstones with dm-thick intercalations of dark grey sandstones.

Member B is composed of mottled yellowish silty mudstones (Fig. 2d) with abundant land plant debris, leaves and root casts. Two brown to blackish indurated beds are present (Fig. 2b), corresponding to homogeneous mudstones alternating with cm-thick graded sandstones with an erosional basal contact. Three lenticular conglomeratic layers are interbedded with the yellowish mudstones (Fig. 2b, e). They are composed of rounded and smoothed pebbles of selenitic gypsum and Alpine metamorphic rocks and are interpreted as fluvial deposits (Colombero et al., 2013). A diverse terrestrial vertebrate fauna is found in the lowermost conglomeratic layer including disarticulated remains of amphibians, reptiles, birds, large herbivores and carnivores (Sardella, 2008; Colombero et al., 2013). In addition, in situ articulated skeletal remains of a single individual of a gomphotheriid, a large elephant-like proboscidean, were found in the yellowish mudstones below the lowermost conglomeratic layer (Colombero et al., 2013). Disarticulated bones and otoliths of coastal marine benthic fish have also been reported occurring with the terrestrial vertebrate fauna: one attributed to the benthopelagic, euryhaline *Aphanius crassicaudus* and one of an undetermined species of *Lophiiformes* (Carnevale et al., 2018).

Member C is composed of grey laminated mudstones with intercalated lenticular dark grey layers (Fig. 2f). In thin section, member C mudstones appear strongly bioturbated (Fig. 3d). Burrows are filled with sand typified by high contents of benthic and planktic foraminifers (Fig. 3e). Three dark grey layers (Figs. 2b, 3c) contain plant remains (leaves, wood fragments), which are particularly abundant and well exposed in the uppermost of the three dark layers (sample LM13; Figs. 2f). Cm-sized rounded nodules surrounded by circumgranular cracks are observed under the microscope (Fig. 3f). Member C is overlain by the lower Zanclean open marine deposits of the AAF (Fig. 2b). The contact is marked by a dm-thick dark-grey arenitic layer (Fig. 2g), reported from other sites of the Piedmont Basin as well (Moncucco; Trenkwalder et al., 2008; Violanti et al., 2011; Narzole borehole; Sturani, 1976; Violanti et al., 2009). In the Pollenzo section, burrows of *Thalassinoides* were recognized at the contact between the dark arenitic layer and the AAF (Dela Pierre et al., 2016).

5.2. Paleontological content

5.2.1. Ostracods

Ostracods (Fig. 5) are first observed at the member A/B transition (Figs. 2b, 4), they disappear in member B and re-appear in member C (Figs. 2b, 4). Here they occur discontinuously in the first ~3.50 m (samples LM1–13), whereas they are ubiquitous in the remaining ~2–3 m below the base of the topmost black layer (Fig. 4). In the lowermost ~3.50 m of member C ostracods mostly consist of fragments of disarticulated valves of *Cyprideis* sp. Fragments could not be selected for $^{87}Sr/^{86}Sr$ analyzes because they are commonly too small to subject them to the cleaning procedure. Similarly, the absence of intact valves hinders the taxonomic classification at the species level. By contrast, in the uppermost ~2–3 m they are well preserved (Fig. 5) and consist of multiple moult stages of both articulated and disarticulated valves, which are diagnostic features of in-situ preservation (e.g. Gliozzi et al., 2007; Cosentino et al., 2012; Stoica et al., 2016; Sciuto et al., 2018).

Overall, two assemblages can be distinguished based on different

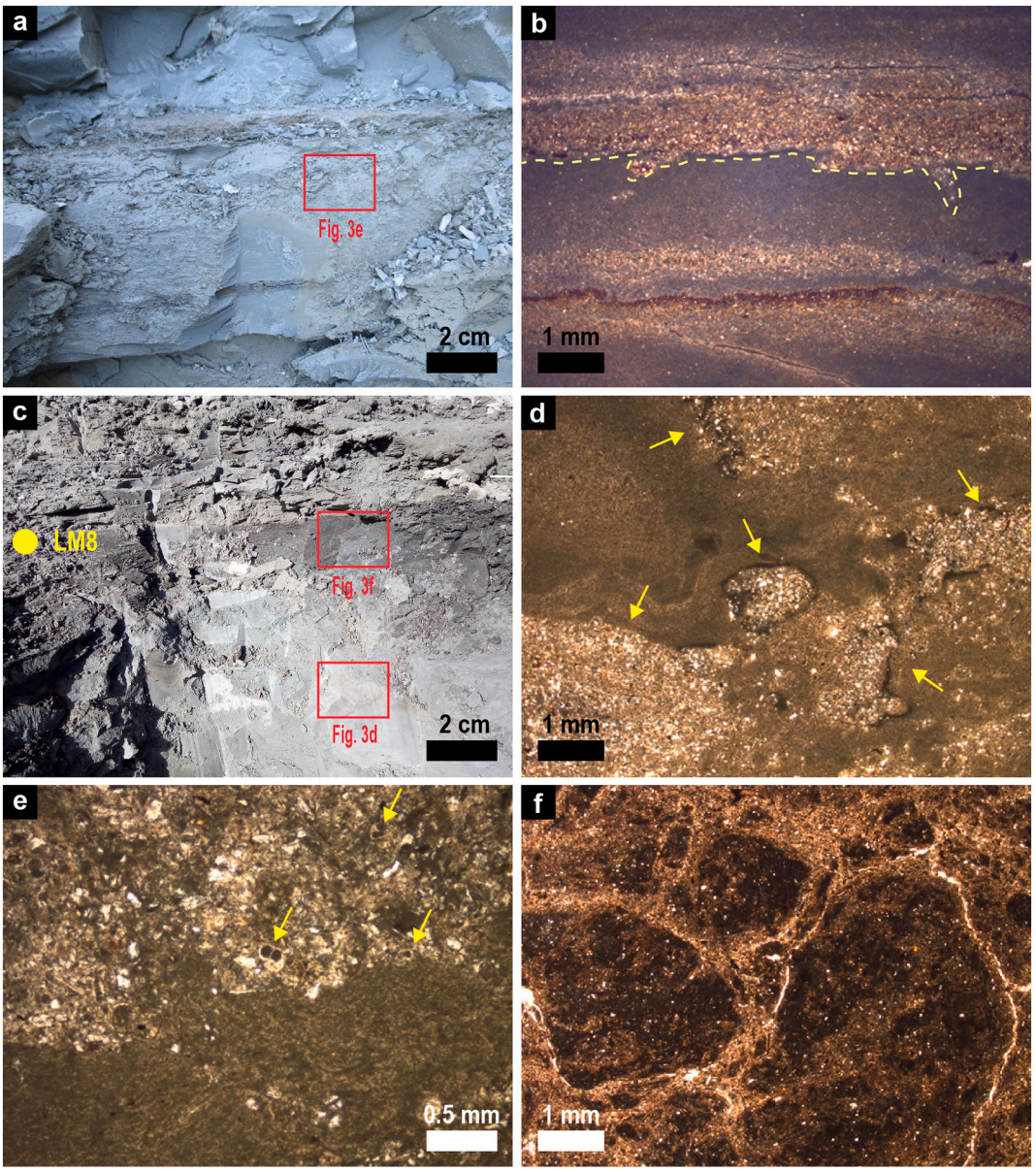

Fig. 3. Field images (a, c) and corresponding transmitted light optical microscope photomicrographs (b, d-f) of the fine-grained sediments of the CSC. **a.** Bedded greyish mudstones of member A; **b.** Graded sandy layers interbedded to homogeneous mudstones. Note the erosional basal contact of the sandy layer (yellow dotted line; sample PA56); **c.** greyish mudstone of member C with, on top, a cm-thick black horizon interpreted as a paleosol; **d.** Member C mudstone with burrows (yellow arrows) filled with fine-grained sand; **e.** Closer view of the fine-grained sand filling the burrows showed in Fig. 3d. Note the abundance of skeletal remains (mostly foraminifera; yellow arrows). Foraminifera tests are possibly filled with pyrite. **f.** Rounded pedogenetic nodules with circumgranular cracks (sample LM8). The cracks are partially filled with calcite. (For interpretation of the references to color in this figure legend, the reader is referred to the web version of this article.)

diversity patterns (Fig. 4). We interpret these assemblages as the Biofacies 1 (low diversity) and Biofacies 2 (high diversity) of Bonaduce and Sgarrella (1999), which are recognized in many other Stage 3 Mediterranean sections (Malaga, Nijar and Vera basins in SE Spain, Bassetti et al., 2006; Guerra-Merchán et al., 2010; Stoica et al., 2016; Apennine basins, Grossi et al., 2008; Cosentino et al., 2012, 2018; Caltanissetta Basin, Grossi et al., 2015; Crete, Cosentino et al., 2007). Biofacies 1 in the Pollenzo section comprises an almost monospecific assemblage of the euryhaline and shallow-water *Cyprideis torosa* with very rare individuals of *Loxoconcha muelleri* (Fig. 4). Well preserved gyrogonites of *Chara* sp. are also observed. Biofacies 1 is found at the member A/B transition and in the lower part of member C (Fig. 4).

In the Pollenzo section Biofacies 2 includes the following species (other than *C. torosa* and *L. muelleri*): *Loxorniculina djafarovi*, *Amnicythere multituberculata*, *Amnicythere propinqua*, *Amnicythere palimpsesta*, *Amnicythere idonea*, *Amnicythere accicularia*, *Cypria* sp., *Tyrrhenocythere ruggierii*, *Tyrrhenocythere pontica*, *Cytherura pirama*, *Camptocypria* sp., *Loxoconcha eichwaldi*, *Loxoconcha kochi*, *Loxocauda limata*, *Zalaniella venusta*, *Euxinocythere (Maeotocythere) praebaquana*, *Hastacandona lotzi* (Fig. 5). Biofacies 2 is recognized only in the two samples taken from the uppermost meter below the black layer at the AAF transition (Fig. 4).

The described ostracod species are only known from the Pontian of the Eastern Paratethys (i.e. Euxinic, Caspian and Dacian basins; Stoica et al., 2013, 2016; Van Baak et al., 2016; Grothe et al., 2018; Lazarev et al., 2020) and the Northern Aegean (Krijgsman et al., 2020 and references therein), where they migrated at ~6.1 Ma from the endorheic Pannonian Basin (Popov et al., 2006; Krijgsman et al., 2010; Grothe et al., 2018). This observation further corroborates the in-situ character of the Biofacies 2 ostracods.

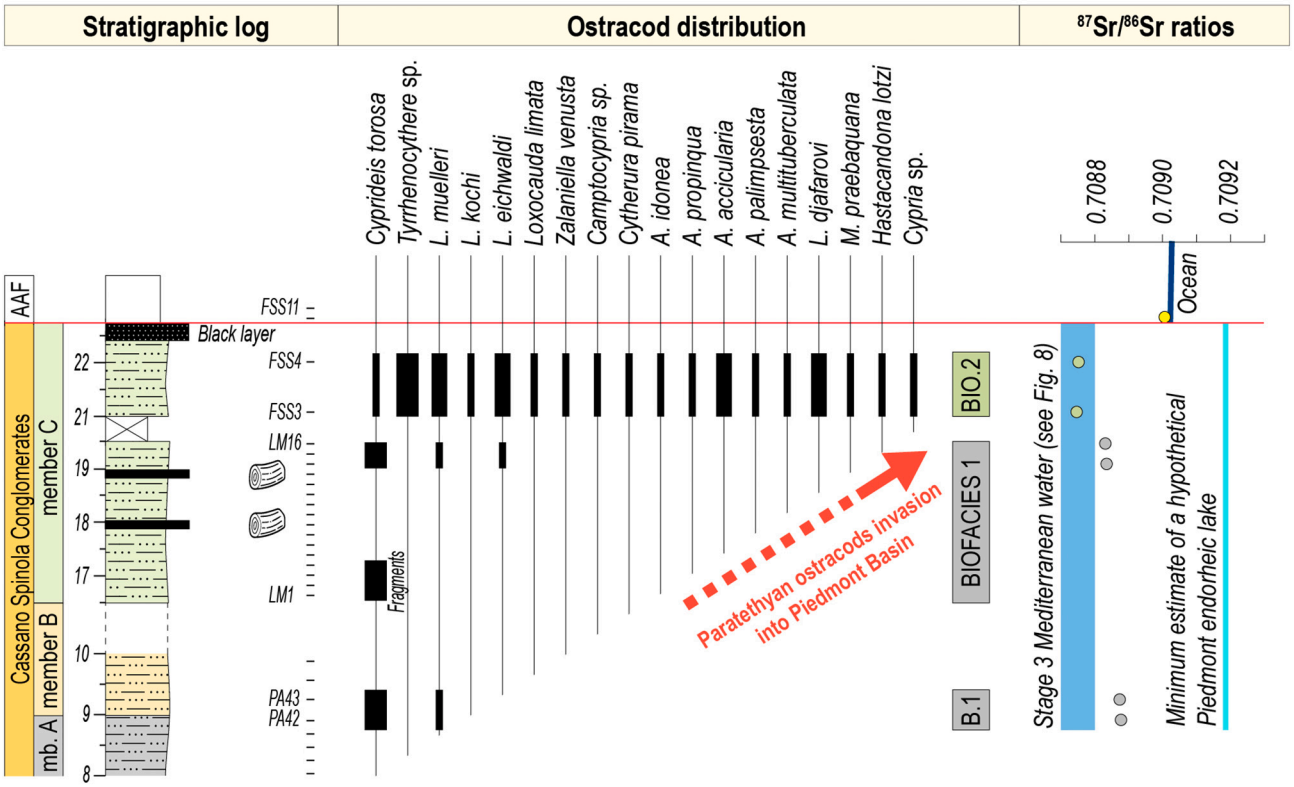

Fig. 4. Ostracod distribution chart along with variations in the $^{87}Sr/^{86}Sr$ ratios measured on ostracod valves. Analytical errors are so small that no error bars are visible at this scale. Note the abrupt increase in ostracod species diversity that typifies the uppermost part of member C. Samples with diversified ostracod assemblages (Biofacies 2) have significantly lower $^{87}Sr/^{86}Sr$ ratios than samples with poorly diversified, *Cyprideis torosa*-dominated assemblages (Biofacies 1). *Tyrrhenocythere ruggierii* and *Tyrrhenocythere pontica* are grouped together in the informal group *Tyrrhenocythere* sp. $^{87}Sr/^{86}Sr$ ratios are plotted against three water sources: (1) average signature of the coeval ocean water (the thickness of the line includes the analytical error; McArthur et al., 2012); (2) minimum estimated signature of a hypothetical lake occupying the Piedmont Basin and corresponding to the $^{87}Sr/^{86}Sr$ ratios of the Po River at its confluence with the Tanaro River (Fig. 1a; see paragraph 6.2 for insights); (3) inferred signature of the water mass filling the Mediterranean Basin during Stage 3 (see paragraph 6.2 for insights).

5.2.2. Foraminifera

Most of the samples collected in the basal member A are barren of foraminifera. Only two samples (PA28 and 42) yield rare small-sized (<125 μm) planktic foraminifera (*Turborotalita quinqueloba*, *T. multiloba*, globigeriniids and few left coiled *Neogloboquadrina acostaensis*). The residues are mostly composed of terrigenous material, typically mica flakes and lithic fragments.

The lowermost sample of member B (PA43; Fig. 2d) is characterized by a reduced content of terrigenous grains and by the presence of mainly planktic foraminifera. Among them, *T. quinqueloba* is most frequent, followed by *T. multiloba*, *Globigerinoides* spp., *Globorotalia scitula* and both left and right coiled *N. acostaensis*. Among the benthic foraminifera, species belonging to the *Bolivina*, *Anomalinoides*, *Oridorsalis*, *Cibicides* and *Uvigerina* genera were observed. The rest of member B is barren of foraminifera or only yields scattered benthic foraminifera in sample PA64.

Samples of the lower part of member C (LM1–3) yield quite diversified foraminifer assemblages, with the planktic component being once again more abundant than the benthic. Among the planktic foraminifera *T. quinqueloba*, *T. multiloba*, *Globigerina bulloides*, *Orbulina universa*, *G. scitula*, *Globorotalia miotumida* and *Globigerinita glutinata* were recognized. *Elphidium*, *Bolivina*, *Bulimina*, *Cibicides*, *Cancris*, *Valvulineria* and *Rectuvigerina* are among the most common benthic taxa. From LM4 upwards foraminifera are generally scattered, except in samples LM10 and LM11, where *T. quinqueloba* is again common and occurs together with rare *T. multiloba* and *G. bulloides*.

The associations that are observed here closely resemble those of the older Sant'Agata Fossili Marls (see Lozar et al., 2010). Some of the common forms found in these assemblages such as *T. multiloba* and *G. miotumida* are thought to have become extinct before Stage 3 (see Lirer et al., 2019). Consequently, it is likely that the foraminifera are reworked. This is supported by the observation that several of the benthic and planktic species are deep-dwelling forms, which is a paleoecological requirement that clearly contrasts with the presence of sedimentological and other micropaleontological features pointing to a shallow and brackish water body during deposition of the CSC (see discussion in paragraph 6.1). *Elphidium* sp. may represent the only exception, being this genus a typical inhabitant of shallow and euryhaline environments that matches with our paleoenvironmental and paleohydrological reconstruction of member C (see discussion in paragraph 6.1). However, since it also frequently found in the SAF (Violanti et al., 2013), reworking cannot be excluded.

5.2.3. Calcareous nannofossils

In all three members, calcareous nannofossil assemblages are made up of both forms clearly reworked because of their biostratigraphic range (Cretaceous, Oligocene and lower-middle Miocene) incompatible with the age of the CSC and taxa which are potentially stratigraphically consistent with the time interval spanned from the CSC and consequently cannot be a priori considered as reworked (Fig. 6). Regrettably, the age-diagnostic taxa *Ceratolithus acutus* (first appearance at 5.36 Ma; Agnini et al., 2017) and *Triquetrorhabdulus rugosus* (last appearance datum at 5.23 Ma; Backman et al., 2012), often reported in late Messinian sediments of both the Mediterranean and Paratethys (Popescu et al., 2017 and references therein) and, therefore, of significant chronostratigraphic and paleoenvironmental implications (see discussion in Andreetto et al., 2021a), have not been found in the CSC of Pollenzo. Quantitative analysis reveals that calcareous nannofossils reworked

Fig. 5. Messinian (Lago-Mare) ostracods from member C of the Cassano Spinola Conglomerates of the Pollenzo section (all pictures are taken on external lateral views, LV-left valve, RV-right valve): 1. *Zalaniella venusta* (Zalányi), LV; 2. *Camptocypria* sp., RV; 3. *Hastacandona lotzi* (Zalányi), LV; 4. *Cypria* sp., RV, juvenile; 5, 6. *Cyprideis torosa* (Jones), 5-LV, female, 6-RV, male; 7. *Tyrrhenocythere ruggierii* (Devoto), RV; 8. *Tyrrhenocythere pontica* (Livental), LV, juvenile; 9, 10. *Amnicythere propinqua* (Livental), RV; 11, 12. *Amnicythere idonea* (Mandelstam, Markova, Rozyeva and Stepanajtys), 11-LV, 12-RV; 13. *Amnicythere palimpsesta* (Livental), RV; 14. *Amnicythere multituberculata* (Livental), LV; 15. *Euxinocythere* (*Maeotocytyhere*) *praebaquana* (Livental), RV; 16. *Amnicythere accicularia* (Olteanu), LV; 17, 18. *Loxoconcha eichwaldi* (Livental), 17-LV, male, 18-LV, female; 19. *Loxoconcha muelleri* (Méhes), LV; 20. *Loxocorniculina djafarovi* (Schneider), LV; 21. *Cytherura pyrama* (Schneider), LV.

from older than late Miocene stratigraphic levels constitute a small percentage (lower than 6%) compared to taxa that are consistent with the age of the CSC. Among these taxa whose stratigraphic distribution is compatible with the age of CSC, the following are observed: *Reticulofenestra antarctica*, *Reticulofenestra haqii*, *Reticulofenestra minuta*, *Reticulofenestra procera, Reticulofenestra pseudoumbilicus, Sphenolitus abies, Sphenolitus moriformis, Helicosphera carteri, Umbilicosphaera jafari, Umbilicosphaera rotula, Calcidiscus leptoporus, Discoaster variabilis, Discoaster brouweri, Coccolithus pelagicus, Toracosphaera, Pontosphaera discopora, Pontosphaera japonica, Pontosphaera multipora, Calcidiscus macintyrei,* and *Syracosphaera pulchra*. Besides *D. variabilis* and *D. brouweri*, other species belonging to the genus *Discoaster* are present. However, they show high degree of fragmentation and recrystallization, hampering their identification at the species level. More in detail, *Reticulofenestra* is by far the most abundant genus, ranging from ~73 to 86% of the total. *R. minuta* makes up more than 38% of the *Reticulofenestra* taxa, followed by *R. haqii* (7–33%, average of 16%), *R. antarctica* (0.5–27%, average of 6%) and *R. procera* (<1%). *Helicosphaera carteri*, *R. pseudoumbilicus*, *C. pelagicus*, *U. jafari* and *Sphenolithus* gr. (herein consisting of *S. abies* and *Strangospora moriformis*; Fig. 6) constitute a minor component (i.e. average abundance between 1 and 5%) of the assemblages. All remaining "age-compatible" taxa occur at abundances <1%.

Calcareous nannofossils assemblages are similar in terms of abundance, (good state of) preservation and taxonomy between the three members and to the older assemblages commonly found in the pre-MSC SAF (Lozar et al., 2010). In member C alone, however, abundant, intact coccospheres were observed. This observation is generally related to conditions of exceptional preservation (e.g. Bown et al., 2014) which, as such, could be indicative of the pristine nature of the member C assemblage (see paragraph 6.1 for a more thorough discussion of the nature of the long-ranging taxa in member C).

The nannofossil associations in the AAF contain the same taxa as in the CSC, with the addition of *Reticulofenestra zancleana*, marker species of the lower Zanclean (Di Stefano and Sturiale, 2010).

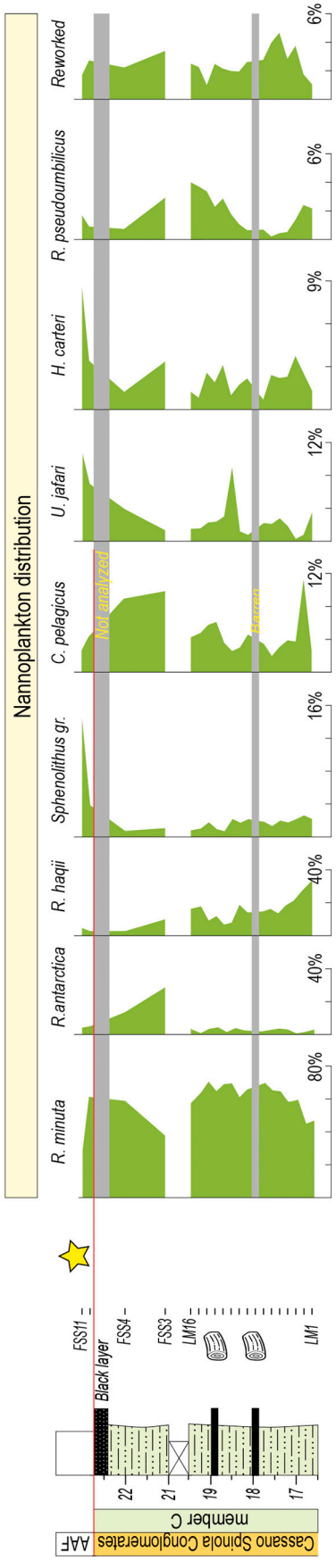

Fig. 6. Relative abundance of dominant calcareous nannofossils taxa in member C of the CSC and at the base of the AAF. *Sphenolithus abies* and *Sphenolithus morjformis* were grouped together in the informal group *Sphenolithus* gr. The yellow star indicates the presence of the age-diagnostic taxon *Reticulofenestra zancleana*. Note changes in scale. (For interpretation of the references to color in this figure legend, the reader is referred to the web version of this article.)

5.2.4. Dinoflagellate cysts

The 18 samples from member C are very rich in pollen grains and organic terrestrial material such as leaf, cuticles, tetrads, fungal spores and woody fragments indicating relatively large amount of terrestrial input. Dinoflagellate cyst (dinocysts) occurrence and diversity vary significantly. Some samples are virtually barren of dinocysts (LM1–9, LM11–13) others show very low abundance and diversity (LM10, LM14–16, FSS3–4). Marine taxa such as *Achomosphera/Spiniferites* spp., *Spiniferites bentori*, *Homotryblium, Operculodinium israelianum, Operculodinium janduchenei* and *Polysphaeridium zoharyi* have been identified. One specimen of *Mendicodinium robustum* has been observed in samples FSS4. This species was informally described from restricted marine and brackish Mediterranean latest middle Miocene-early late Miocene sediments (Zevenboom, 1995). Only one specimen of the Paratethyan species *Caspidinium rugosum* and three specimens of *Spiniferites cruciformis* were identified in sample LM15.

Early Zanclean samples FSS10–11 from the AAF are marked by a large increase in dinocyst abundance and species richness and by remarkable improvement in the dinocyst preservation. The most abundant taxa in sample FSS10 are *Impagidinium patulum*, *Operculodinium* spp., *Lingulodinium machaerophorum* (some specimens with reduced processes), *Spiniferites* spp., *Brigantedinium* spp., *Nematosphaeropsis labyrinthus* and *Reticulatosphaera actinocoronata*, which are known from coastal to (outer) neritic environments. In sample FSS11 *Impagidinium patulum* is dominant and *Nematosphaeropsis labyrinthus, Reticulatosphaera actinocoronata*, *Operculodinium janduchenei* and *Lingulodinium macherophorum* (with fully developed processes) are present. This association reflects an outer neritic/oceanic environment.

In the lower Zanclean samples, marine dinocysts are well preserved, diverse and abundant, all features that corroborate their in-situ character. By contrast, the taxa recognized in member C are often poorly preserved. This makes the identification at the species level and the discrimination of possible in-situ components, for instance, by means of fluorescence microscopy (Pellen et al., 2017; Hoyle et al., 2018), really challenging. The different preservation and abundance of the dinocysts between the lower ~3.5 m of member C (i.e. samples LM1–13) and the base of the AAF allows us to hypothesize that the few dinocysts recovered in the lower part of member C are reworked. By contrast, the subtle increase in the dinocyst preservation and abundance in the uppermost ~3 m (i.e. samples LM14–16, FSS3–4) may point to in-situ deposition.

5.3. $^{87}Sr/^{86}Sr$ ratios

$^{87}Sr/^{86}Sr$ ratios from the CSC range from 0.708871 to 0.708746 (Fig. 4, Table 1). The higher values of 0.708870–0.708871 (PA42–43) and 0.708831–0.708834 (LM 14–15) come from *C. torosa* specimens

Table 1
$^{87}Sr/^{86}Sr$ composition and details of the analyzed samples.

Sample	Lithostr. unit	Age	Species (analyzed material)	$^{87}Sr/^{86}Sr$	2σ (10^{-6})
FSS11	AAF	Early Zanclean	*Orbulina* (10 tests)	0.709006	7.02
FSS4	CSC (member C)	Late Messinian	*T. ruggierii* (6 adult valves)	0.708752	5.48
FSS3	CSC (member C)	Late Messinian	*T. ruggierii* (6 adult valves)	0.708746	5.28
LM15	CSC (member C)	Late Messinian	*C. torosa* (6 adult valves)	0.708831	6.05
LM14	CSC (member C)	Late Messinian	*C. torosa* (6 adult valves)	0.708834	5.18
PA43	CSC (member A)	Late Messinian	*C. torosa* (6 adult valves)	0.708871	3.628
PA42	CSC (member A)	Late Messinian	*C. torosa* (6 adult valves)	0.708870	4.325

forming the oligotypic Biofacies 1 (Fig. 4). Instead, the lower values of 0.708746 (FSS3) and 0.708752 (FSS4) come from *T. ruggierii* specimens forming the more diversified Biofacies 2 (Fig. 4). In contrast with the CSC data where the $^{87}Sr/^{86}Sr$ ratios are substantially lower than Messinian ocean water, $^{87}Sr/^{86}Sr$ at the base of the AAF (0.709006) are close to the global ocean Sr curve for the lowermost Pliocene (McArthur et al., 2012), but still outside its error range (Fig. 4).

6. Discussion

6.1. Paleoenvironmental evolution of the Piedmont Basin during Stage 3

Our newly acquired sedimentological and paleontological data, together with previously published results from both Pollenzo and other localities in the Piedmont Basin, say little about the duration of Stage 3 in Pollenzo because of the lack of chronological controls, but they reveal that at least three distinct environmental conditions occurred during the here recorded time slice of Stage 3.

6.1.1. Member A

The fine-grained and thinly laminated deposits of member A (Fig. 2c) reflect deposition in a low-energy subaqueous environment after a period of tectonic-driven basin instability resulting in the deposition of the VVC (Fig. 7a). The absence of in-situ fauna and bioturbation throughout most of member A may suggest that the oxygen content was low. Only in the uppermost part of member A, the presence of abundant

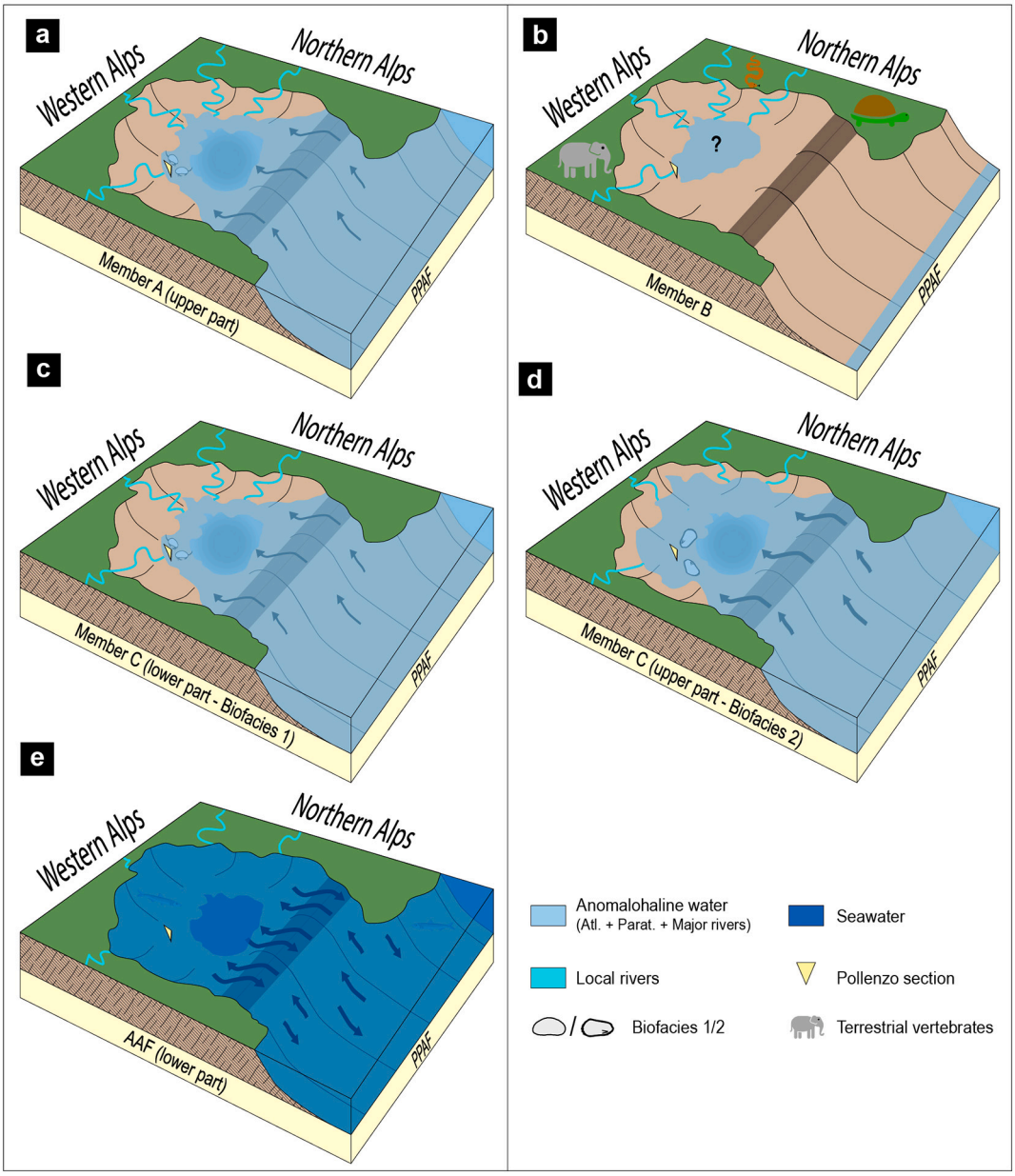

Fig. 7. Evolution through part of MSC Stage 3 of the Piedmont Basin related to base-level variations in the open Mediterranean Basin. **a.** A shallow-water subaqueous environment establishes in the Alba region after the emplacement of the VVC. **b.** Falling stage of the Mediterranean base level, witnessed by the spreading of continental conditions. **c.** The rising Mediterranean base-level establishes, in the Pollenzo area, a shallow-water environment inhabited by *C. torosa* with higher, more local river-like $^{87}Sr/^{86}Sr$ ratios. **d.** The ongoing transgression causes a deepening and freshening in the Piedmont Basin, setting up the environmental conditions for the truly Paratethyan ostracods to thrive. The increased contribution of Mediterranean waters with lower $^{87}Sr/^{86}Sr$ ratios than the local rivers causes a lowering of the $^{87}Sr/^{86}Sr$ ratio of the water mass. **e.** Changes in the Mediterranean-Atlantic gateway configuration re-establish a normal marine environment at the base of the Zanclean.

C. torosa, which is known today to be a shallow-water dweller (up to 30–50 m of depth, optimum around 7 m; Neale, 1988; Meisch, 2000; Meyer et al., 2016), indicates a shallow-water paleoenvironment at Pollenzo (i.e. <10–30 m deep). Instead, little can be said about the paleosalinity: both *C. torosa* and charophytes can withstand and thrive in a very wide range of aquatic environments and salinity (Pełechaty et al., 2013; Grossi et al., 2015; De Deckker and Lord, 2017 and references therein). The Moncucco section (Fig. 1b) located in the northern side of the Piedmont Basin (Torino Hill; Fig. 1a–b) may provide an estimation of paleosalinity during deposition of the topmost part of member A. At Moncucco, a poorly diversified ostracod assemblage is found in mudstones resting just below mammal-rich sediments (Angelone et al., 2011) likely referable to member B (see below). Besides *Cyprideis,* identified at the species level as *Cyprideis agrigentina* by Angelone et al. (2011), and *L. kochi,* some specimens of *A. propinqua* are also found (Angelone et al., 2011). This species is reported to have depth ranges compatible with those of *C. agrigentina* and L. *kochi*, but stricter salinity requirements, which has to stay within the oligo-mesohaline field (3–14‰; Gliozzi and Grossi, 2008). These findings therefore suggest that the shallow-water paleoenvironment depositing member A was typified by brackish conditions. Fine-grained deposits similar to those of member A of Pollenzo are also reported on top of the VVC in cores that penetrated the CSC in the Alessandria and Savigliano depocenters (Fig. 1a; Ghielmi et al., 2019). In contrast, member A mudstones are absent in localities further away from the deepest sectors both to the S and to the N, where the erosional surface capping the VVC is directly overlain by the AAF (e.g. Monregalese area; Ghielmi et al., 2019).

6.1.2. Member B

The transition from the grey shales of member A to yellowish mudstones of member B (Fig. 3c) with rhizoliths, terrestrial mammals (Colombero et al., 2013) and three conglomerate beds (Fig. 2b, e) with typical features of fluvial transport demonstrates the basinward shift of the coastline and the establishment, at Pollenzo, of a recurrently dried alluvial plain crossed by a fluvial network and surrounded by a variety of continental environments (grasslands, woody areas, rocky habitats; Fig. 7b). These continental environments provided a corridor for migrating mammals from mainland Europe into the Italian peninsula (Sardella, 2008; Angelone et al., 2011). The occurrence of Alpine metamorphic pebbles in the conglomerates indicate that the Alpine chain was already partially emerged during deposition of the member B and it was undergoing intense erosion. Scattered brownish to black shaley lenses intercalated with the yellowish pelites (Fig. 2b) are possibly indicative of ephemeral, marshes that punctuated the alluvial plain. Sediments similar to the ones attributed, in Pollenzo, to member B, and rich in mammal fossils, freshwater and continental gastropods (Angelone et al., 2011; Colombero et al., 2014, 2017; Harzhauser et al., 2015; Grunert et al., 2016) are also found in the Moncucco section. This suggests that continental conditions involved a larger sector of the Piedmont Basin than only the Alba region (Fig. 7b).

6.1.3. Member C

The transition from the continental deposits of member B to the grey laminated mudstones of member C indicates the renewal of a subaqueous environment. Additionally, they are interbedded with dark silty layers (Fig. 2c–d) with cm-sized rounded nodules surrounded by circumgranular cracks (Fig. 3h), which we interpret to possibly represent immature paleosols. Overall, these features indicate that member C is the sedimentary expression of a shallow water body with a fluctuating base-level responsible for periodic subaerial exposure. The amplitude of the fluctuations was probably rather small (<30 m), based on the shallow-water mode of life of the ostracod *C. torosa* which, albeit discontinuously, dominates the benthic assemblages for most of member C (Fig. 4). In the uppermost 1–2 m before the topmost black layer, the ostracod assemblages are highly diverse, dominated by Paratethyan species (Fig. 5) and relatively impoverished in *C. torosa* (Fig. 4). This assemblage is similar to that of the Moncucco section (Fig. 1a; Trenkwalder et al., 2008) and other Messinian Mediterranean successions (e.g. Cosentino et al., 2007, 2012, 2018; Grossi et al., 2008; Guerra-Merchán et al., 2010; Stoica et al., 2016; see Andreetto et al., 2021a for further references). According to the paleoecological analyzes carried out by Gliozzi and Grossi (2008) on the Paratethyan ostracods, the stacking of Biofacies 2 over Biofacies 1 in the uppermost ~2 m (Fig. 4) indicates a deepening- and freshening-upward trend. Paratethyan ostracods, however, occur with the diverse calcareous nannofossil assemblages (which include intact coccospheres) dominated by *Reticulofenestra* and subordinate specimens of *H. carteri*, *C. pelagicus*, *Sphenolithus abies* and *Umbilicosphaera jafari* (Fig. 6).

The co-occurrence of calcareous nannofossils with Paratethyan organisms in the same sediments raises a concern, which is not new in Stage 3 studies (e.g. Cita et al., 1978; Bertini, 2006; Popescu et al., 2007; Roveri et al., 2008a; Cosentino et al., 2012; Pellen et al., 2017; Caruso et al., 2020). Marine microfossils have paleoecological requirements apparently incompatible with those of the Paratethyan ostracods: following the paleoenvironmental significance of the MSC ostracod assemblages proposed by Gliozzi and Grossi (2008), Biofacies 2 is indicative of an oligo-mesohaline environment (0.5–18 g/l; The venice system for the classification of marine waters according to salinity, 1958); instead, calcareous nannofossils are generally adapted to higher, oceanic salinities typically ranging between 33 and 37 g/l. On this basis, and considering that Paratethyan ostracods are certainly in-situ (e.g. Gliozzi et al., 2007; Stoica et al., 2016; Sciuto et al., 2018; Caruso et al., 2020; Andreetto et al., 2021a), the marine microfossils in Stage 3 sediments are generally considered to be reworked. However, some calcareous nannoplankton today bloom sufficiently intensively to dominate the phytoplankton assemblage in basins where oligo-mesohaline conditions are seasonally or permanently established. Examples include the Black Sea (Giunta et al., 2006), Baltic Sea (Hällfors, 2004; Thomsen, 2016), Adriatic Sea (Skejić et al., 2021) and Thessaloniki Bay (Dimiza et al., 2020). These studies of calcareous nannoplankton in modern, low salinity marine environments therefore do not preclude the coexistence of brackish Paratethyan ostracods and marine calcareous nannofossils in member C. Those species that have been identified here as potentially in-situ (see Fig. 6) are largely accepted to be adaptable to lower than normal marine salinity and to thrive during times of strongly fluctuating environmental conditions (Wade and Bown, 2006; Auer et al., 2014). In particular, *R. minuta*, which accounts for up to 70% of the assemblages of member C (Fig. 6), is considered a hardy, opportunistic and euryhaline taxon capable of withstanding highly stressed environments (Wade and Bown, 2006 and references therein). If Wade and Bown (2006) and Auer et al. (2014), among others, are correct in their hypothesis that *R. minuta* and the other nannotaxa listed in Fig. 6 can occur in low-salinity environments, then member C of the Pollenzo section documents that the Piedmont Basin was, during its deposition, exchanging water with the rest of the Mediterranean Basin via the Po Plain-Adriatic Foredeep (PPAF; Figs. 7c-d), which in turn was being simultaneously supplied by the Atlantic seawater other than Eastern Paratethys brackish water.

In-situ assemblages of calcareous nannofossils including the most abundant taxa recognized in the CSC have already been reported by Popescu et al. (2007) and Pellen et al. (2017) in Stage 3 sediments from more southerly localities in the Adriatic region (i.e. Monticino, Maccarone, Civitella del Tronto, Fonte dei Pulcini and Fonte della Casa). The evidence used to argue that the nannofossils were in situ was the presence of rare *Ceratolithus acutus* and *Triquetrorhabdulus rugosus*. These are biostratigraphic markers of the uppermost Messinian/early Zanclean (Di Stefano and Sturiale, 2010; Agnini et al., 2017) and, therefore, cannot be reworked from older sediments. However, neither Roveri et al. (2008b) nor Cosentino et al. (2012) identified these age-diagnostic taxa in the same sections and they have also not been found by us in the CSC of the Piedmont Basin. We therefore suggest that taphonomic and paleoecological evidence, rather than biostratigraphic criteria, should be used in

the interpretation of calcareous nannoplankton assemblages in Stage 3 sediments.

Occurring with the Biofacies1–2 ostracods in the upper part of member C are also low diversity marine dinocyst assemblages, which include *Achomosphera/Spiniferites* spp., *Spiniferites bentori*, *Homotryblium*, *Operculodinium israelianum*, *Operculodinium janduchenei*, *Polysphaeridium zoharyi* and one specimen of *Mendicodinium robustum*. Although these assemblages are of difficult interpretation due to their extremely poor preservation, their sudden appearance in concomitance with the ostracods may suggest that they were transported into the Piedmont Basin from the same water mass. In agreement with the environment indicated by the taxa of potentially in situ calcareous nannofossils, the occurrence of these dinocyst taxa known to inhabit restricted shallow marine, lagoonal settings (Pross and Brinkhuis, 2005; Zonneveld et al., 2013) is reconcilable with the presence of the ostracods.

The black layer capping member C (Fig. 2g) and marking the paleohydrological change from brackish to normal marine salinity conditions shares a very similar sandy texture and black color with other dark beds found in the CSC (Fig. 2c–d). Similar black layers found just below the lowermost Zanclean sediments in a number of localities of the Northern-Central Apennines (Gennari et al., 2008) and in the Cypriot Pissouri Basin (Rouchy et al., 2001) have also been interpreted as paleosols. However, the presence of *Thalassinoides*, which are marine firm ground burrows today constructed by a variety of marine organisms (Myrow, 1995), at the top of the topmost black layer of the Piedmont Basin (Dela Pierre et al., 2016) may be indicative that at least part of it was deposited under marine conditions. However, more detailed sedimentological, geochemical and paleontological investigations are required to fully confirm its paleoenvironmental significance.

6.2. *Episodic establishment of water exchange between the Piedmont Basin and the Mediterranean during Stage 3*

Sr^{2+} cations in solution and absorbed by Ca^{2+}-bearing minerals during precipitation have an $^{87}Sr/^{86}Sr$ ratio that results from the integration of Sr^{2+} from isotopically-different and variably-concentrated water sources flowing into the basin. As long as the $^{87}Sr/^{86}Sr$ fingerprint of these sources is known, then the hydrologic fluxes to the basin can be reconstructed (e.g. Doebbert et al., 2014; Reghizzi et al., 2018; Andreetto et al., 2021b). This methodology is only applicable to continental environments (lakes and rivers) or sedimentary basins which have a restricted connection with the global ocean (like the Mediterranean Basin during the MSC; Roveri et al., 2014a). Continental inputs are, in fact, not distinguishable in normal oceanic settings (e.g. Kuznetsov et al., 2012; Benito et al., 2021) due to the far higher Sr concentration in seawater (7.8 mg/l; Palmer and Edmond, 1992) than in river water (<<1 mg/l; Palmer and Edmond, 1992; Gaillardet et al., 1999; Marchina et al., 2018). $^{87}Sr/^{86}Sr$ ratios from the CSC (0.708834–0.708746) are significantly lower than those of the coeval seawater (~0.709024; McArthur et al., 2012). These data strongly indicate that sedimentation of member A and C mudstones took place in a subaqueous environment exclusively (endorheic lake) or mainly (lagoon connected to the external sources via the Mediterranean) formed by non-marine inputs. If this water body was an endorheic lake, like suggested by Amadori et al. (2018), then the $^{87}Sr/^{86}Sr$ value of the Paratethyan ostracod valves must be representative of the $^{87}Sr/^{86}Sr$ ratio of the lake water, which is the product of all the river(s) flowing into the lake (e.g. Joordens et al., 2011; Baddouh et al., 2016) after the weathering and erosion of the isotopically-different, catchment-forming lithologies (e.g. Palmer and Edmond, 1992; Brenot et al., 2008; Hajj et al., 2017; Marchina et al., 2018; Peucker-Ehrenbrink and Fiske, 2019).

The presence, in member B, of pebbles of metamorphic rocks exposed in the Alpine chain today indicates that the bedrocks forming the proto-Alps were a source of Sr^{2+} ions into the Piedmont Basin. Measurements of the Sr signatures of the rivers that flowed into the Piedmont Basin during MSC Stage 3 are obviously not available, but can be reliably approximated assuming that the paleorivers had similar $^{87}Sr/^{86}Sr$ ratios to those of the present-day rivers (e.g. Vasiliev et al., 2010, 2021; Placzek et al., 2011; Doebbert et al., 2014; Grothe et al., 2020) because the catchments of modern rivers of the Mediterranean area, including the Piedmont region, did not change significantly since the latest Messinian (e.g. Brass, 1976; Goudie, 2005; Schildgen et al., 2014; Cosentino et al., 2018). $^{87}Sr/^{86}Sr$ data are available for all major rivers draining Northern Italy today (Marchina et al., 2018). Among them, only the $^{87}Sr/^{86}Sr$ data of the longest river in Northern Italy, the Po River, are chosen as the local reference $^{87}Sr/^{86}Sr$ signal because the Po River integrates at its mouth and, along its course, via its tributaries, the dissolved solutes provided by the lithologies forming the Alps and Apennines, were the catchments are located (Marchina et al., 2018). The $^{87}Sr/^{86}Sr$ composition at any given point of the Po River course is therefore representative of the mixing of isotopically-different Sr^{2+} coming from all the lithologies outcropping in the catchments upstream of that point.

We consider the lowest $^{87}Sr/^{86}Sr$ ratio of the Po River before its confluence with the Tanaro River (i.e. 0.709187; Fig. 1a, which occurs approximately at the far eastern border of the Piedmont Basin (Fig. 1a), as the minimum estimate of the $^{87}Sr/^{86}Sr$ isotope composition of a lake that could have hypothetically existed in the late Messinian Piedmont Basin. The $^{87}Sr/^{86}Sr$ values measured for the Po water at six locations before confluence with the Tanaro River range between 0.709187 and 0.709745 (Fig. 8). These values are compatible with the mixing of high radiogenic Sr^{2+} provided by the igneous and metamorphic rocks forming the great majority of the Alpine sector with less radiogenic Sr^{2+} released by Jurassic ophiolites and Mesozoic carbonates locally outcropping along the course of the tributaries Dora Baltea and Tanaro (Fig. 1a; see Dal Piaz, 2010 for insights into the geology of Northern Italy). This range of values, however, is substantially higher than the $^{87}Sr/^{86}Sr$ values measured on ostracods valves from both the member A/B transition (0.708870–0.708871) and from member C (0.708746–0.708834; Figs. 4, 8, Table 1). Another possibility, if the Piedmont Basin had in the latest Messinian an areal extent and/or an arrangement of the fluvial network different than today, would be that tributaries of the Po River further east of the Tanaro River also supplied Sr^{2+}. Even if so, at no point beyond the present-day eastern margin of the Piedmont Basin the Po River attains $^{87}Sr/^{86}Sr$ values low enough that overlap with the ostracod data (Fig. 8). This includes its lower reaches where, compared to the upper reaches, there is a higher contribution of water that drains carbonates and that gives some of the northeastern Po tributaries lower $^{87}Sr/^{86}Sr$ ratios (Marchina et al., 2018). Consequently, the $^{87}Sr/^{86}Sr$ ratios from the present-day rivers of Northern Italy do not support the notion that the biota of the CSC inhabited an endorheic lake fed by northern Italian rivers (e.g. Amadori et al., 2018). Instead, $^{87}Sr/^{86}Sr$ ratios measured on Stage 3 Piedmont ostracods must be accounted for by mixing of local freshwaters with their relatively high $^{87}Sr/^{86}Sr$ signatures with water derived from an external source and carrying Sr^{2+} cations with a lower $^{87}Sr/^{86}Sr$ ratio (Fig. 7a, c–d).

A similar disparity between high $^{87}Sr/^{86}Sr$ ratio river water and low $^{87}Sr/^{86}Sr$ ratios measured on Stage 3 ostracods was found to occur also in the Sorbas-Nijar-Vera basins in SE Spain (Fig. 8; Andreetto et al., 2021b). These Spanish data were interpreted to reflect a combination of (local) fluvial and Mediterranean input, which is thought to have had, at times during MSC Stage 3, a $^{87}Sr/^{86}Sr$ signature sufficiently low to draw the higher ratios of the Spanish rivers down to the values acquired by the ostracods (Andreetto et al., 2021b). $^{87}Sr/^{86}Sr$ values measured on gypsum and ostracod valves from more central Mediterranean basins, far from the influence of the local fluvial input during the highstand phases and where waters from the lower radiogenic large rivers (e.g. Nile: 0.7060, Brass, 1976; Rhône: ~0.7087, Albarède and Michard, 1987 and Gaillardet et al., 1999) and Eastern Paratethys (0.70840.7085, Grothe et al., 2020) and the higher radiogenic Atlantic Ocean (~0.709024;

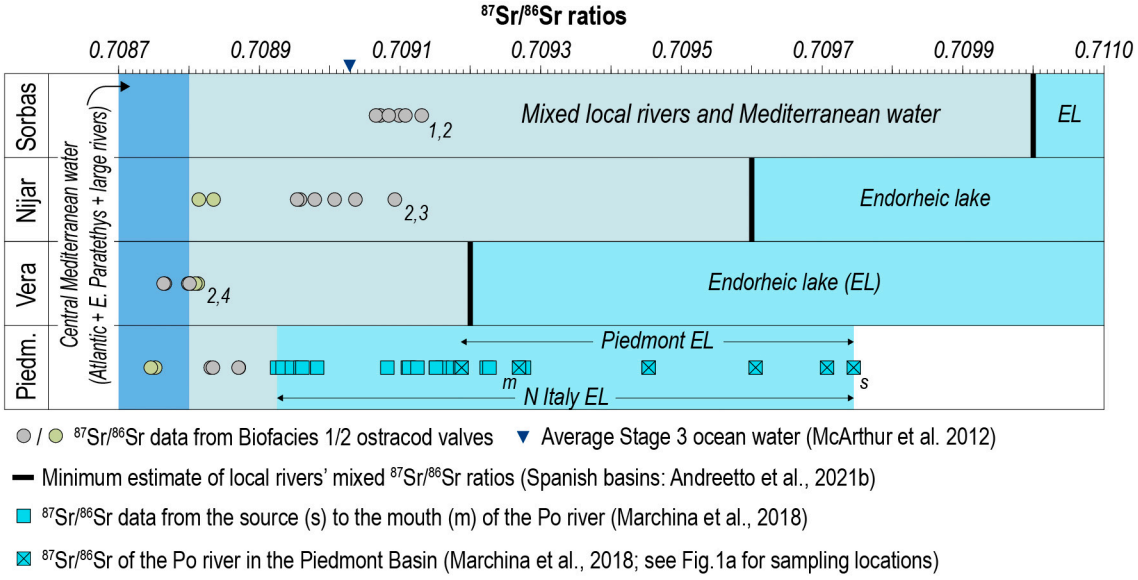

Fig. 8. Comparison between the Stage 3 $^{87}Sr/^{86}Sr$ record of the Piedmont Basin and that of the marginal basins of SE Spain (1: McCulloch and De Deckker, 1989; 2: Andreetto et al., 2021b; 3: Roveri et al., 2019; 4: Fortuin et al., 1995). $^{87}Sr/^{86}Sr$ ratios are plotted against the $^{87}Sr/^{86}Sr$ fingerprint of the water mass filling the Mediterranean during Stage 3 (Andreetto et al., 2021b), the coeval seawater signature (McArthur et al., 2012) and the estimated range of $^{87}Sr/^{86}Sr$ ratios for isolated lakes. Note that none of the $^{87}Sr/^{86}Sr$ ratios measured on Biofacies 1 and 2 ostracods from four separated marginal basins overlap with the $^{87}Sr/^{86}Sr$ signature expected from endorheic lakes (see paragraph 6.2 for insights).

McArthur et al., 2012), were coming together (e.g. Manzi et al., 2009; Roveri et al., 2014c; Marzocchi et al., 2016; Vasiliev et al., 2017; García-Veigas et al., 2018), are consistently lower than 0.708850 (Andreetto et al., 2021b). We therefore suggest that the $^{87}Sr/^{86}Sr$ Piedmont CSC data are also the consequence of mixed fluvial and Mediterranean input (Fig. 8). For this to be the case, the Mediterranean water level must have been full enough to reach the Piedmont Basin and have been dominated by non-marine water (e.g. Manzi et al., 2009, 2016; Roveri et al., 2014b, 2014c; Marzocchi et al., 2016; Stoica et al., 2016; Pellen et al., 2017; Vasiliev et al., 2017; García-Veigas et al., 2018), at least during times when Paratethyan ostracods were colonizing the marginal basins (e.g. Andreetto et al., 2021b).

6.3. *Towards the marine replenishment of the Piedmont Basin*

The upper part of member C comprises a stratigraphic increase in ostracod diversity. The poorly diversified, shallower Biofacies 1 is associated with higher river-like ratios, whereas the deeper water, more diverse Biofacies 2 has lower ratios, similar to those that characterize the Stage 3 Mediterranean water (Fig. 4). This decrease in $^{87}Sr/^{86}Sr$ in the upper part of member C is likely to reflect an enhanced contribution of Mediterranean water to the Piedmont Basin in parallel with increased water depth.

The ambiguous nature of the topmost black layer at the M/P boundary (Fig. 2g) hampers the interpretation of this transition both at Piedmont and Mediterranean-wide. For the Zanclean transgression to have been catastrophic (e.g. Micallef et al., 2018; Caruso et al., 2020; Garcia-Castellanos et al., 2020; Spatola et al., 2020), the black layer would need to have been deposited during a regression following the rising Mediterranean base-level documented in the upper part of member C. The alternative, non-catastrophic M/P transition would instead require rising Mediterranean base-level to have continued into the Pliocene uninterrupted.

Notwithstanding the nature of the transition, the Pliocene AAF sediments only contain stenohaline marine taxa, including some biostratigraphic markers of the early Zanclean such as the nannofossil *Reticulofenestra zancleana* (Di Stefano and Sturiale, 2010). This indicates that early Pliocene sedimentation in Piedmont took place under open marine conditions (Fig. 7e). The dinocyst association in AAF samples FSS10 and FSS11, 30 and 35 cm above the M/P boundary, reflects a deepening-upward trend from coastal/(outer) neritic to outer neritic/oceanic environments. The proportion of deep bathyal foraminifera and ostracod taxa in Lower Zanclean samples from the Narzole core (Figs. 1a-b) suggests that the Early Zanclean bathymetry was ~500–700 m in the Pollenzo area (Violanti et al., 2009). Similar Early Zanclean faunal associations have previously been described from the AAF exposed in the Piedmont Basin (Sturani, 1973; Trenkwalder et al., 2008; Violanti et al., 2011) and basal Pliocene sediments elsewhere in the Mediterranean (e.g. Castradori, 1998; Iaccarino et al., 1999; Rouchy et al., 2003, 2007; Gennari et al., 2008; Guerra-Merchán et al., 2014; Corbí and Soria, 2016; Corbí et al., 2016; Frigui et al., 2016; Roveri et al., 2019; Caruso et al., 2020). These have also been interpreted as indicating that Atlantic waters had fully replenished the Mediterranean by 5.332 Ma. The $^{87}Sr/^{86}Sr$ of Early Zanclean microfossils should therefore be within error of ocean ratios. The $^{87}Sr/^{86}Sr$ ratio is homogeneous in the global ocean (McArthur et al., 2012) and in semi-closed basins with an unrestricted oceanic gateway (e.g. Kuznetsov et al., 2012). The $^{87}Sr/^{86}Sr$ ratio measured on *Globigerina* tests (0.709006 ± 0.00000702) 35 cm above the base of the AAF (sample FSS11) is significantly higher than the CSC samples below it and is close to, but analytically lower than the coeval ocean value (~0.709024 ± 0.000004; McArthur et al., 2012; Fig. 4). Model calculations from Topper et al. (2014) show that $^{87}Sr/^{86}Sr$ values measurably deviate from oceanic values towards riverine values if the river-derived Sr flux constitutes at least 25% of the total water flux. These conditions are more likely to be achieved when the connection between the ocean and the marginal basin is restricted (Topper et al., 2014). We suggest that this discrepancy reflects the delayed response of the system to the hydrological change occurring at the M/P boundary, with substantial amounts of non-marine Sr^{2+} still circulating in the depositional environment. This geochemical evidence that fully marine conditions were not restored in Piedmont immediately after the Zanclean replenishment is mirrored by a higher resolution Zanclean Sr isotope dataset from the Adana Basin (Southern Turkey; Cipollari et al., 2013). Elsewhere in the Mediterranean (e.g. Chelif Basin in Algeria and the deep Alborán Basin; Rouchy et al., 2007; Bulian et al., 2021), some authors have reported low diversity

foraminiferal assemblages that are consistent with a delay to the establishment of fully marine conditions in the lowermost Pliocene. The distribution of these data across both East and Western Mediterranean basins indicates that the delay in establishing fully marine conditions was at a Mediterranean scale, rather than a local phenomenon. It was estimated that such conditions possibly lasted for at least half of a precession cycle after the M/P transition (e.g. Pierre et al., 2006; Rouchy et al., 2007), but accurate chronological data showing the exact time at which normal marine fossil assemblages and geochemical signals returned in the Mediterranean are still lacking.

7. Conclusions

Our cross-disciplinary study of the Cassano Spinola Conglomerates in the marginal Piedmont Basin provides new multifaceted insights on Stage 3 of the Messinian Salinity Crisis. The Piedmont Basin remained underwater possibly for most of Stage 3, hosting an inhospitable subaqueous environment (member A) that only before being superseded by continental conditions (member B) gets populated mostly by the ostracod genus *Cyprideis* and shows evidence in the $^{87}Sr/^{86}Sr$ ratios that was exchanging water with the Mediterranean. At some point this environment shrinks from the more marginal areas of the basin, exposing terrestrial pathways for trans-European mammal migrations. The abrupt replacement of continental deposits by subaqueous mudstones (member C) provides evidence for a transgression. This event is accompanied by the appearance of progressively more diverse assemblages of Paratethyan ostracods possibly together with taxa of calcareous nannofossil and dinocysts adaptable to environments with lower than seawater salinity and fluctuating environmental conditions. $^{87}Sr/^{86}Sr$ ratios of the latest Messinian ostracods infer a mixture of local river and central Mediterranean waters, which demonstrate that the Piedmont Basin was already connected with the central Mediterranean water mass before the M/P boundary. The ostracods' diversity change observed at the top of the CSC matches with the decrease in $^{87}Sr/^{86}Sr$ ratios from higher to lower values and together they reflect a progressive upward increase of the depth and freshening of the environment that we relate to the enhanced entrance of Mediterranean water in a general framework of Mediterranean base-level rise. When placed in a more regional context, our results indicate that the Mediterranean Basin was relatively full of water derived from Atlantic, Eastern Paratethys and the ever-flowing large rivers at times corresponding to Paratethyan ostracod colonization of the rims.

Data availability

A complete description of the procedures followed for thin section preparation, paleontological and $^{87}Sr/^{86}Sr$ isotope analyzes is provided as Supplementary data (File S1). Raw counts and percentages of the calcareous nannofossils are also provided in separate spreadsheets (File S2).

Declaration of Competing Interest

The authors whose names listed immediately below certify that they have NO affiliations with or involvement in any organization or entity with any financial interest (such as honoraria; educational grants; participation in speakers' bureaus; membership, employment, consultancies, stock ownership, or other equity interest; and expert testimony or patent-licensing arrangements), or non-financial interest (such as personal or professional relationships, affiliations, knowledge or beliefs) in the subject matter or materials discussed in this manuscript.

Author names: Federico Andreetto, Alan Maria Mancini, Rachel Flecker, Rocco Gennari, Jamie Lewis, Francesca Lozar, Marcello Natalicchio, Francesca Sangiorgi, Marius Stoica, Francesco Dela Pierre, Wout Krijgsman.

Acknowledgments

This research was supported by the project SALTGIANT-Understanding the Mediterranean Salt Giant, a European project which has received funding from the European Union's Horizon 2020 research and innovation program, under the Marie Sklodowska-Curie [grant agreement No 765256]. This manuscript benefited from the comments of two anonymous reviewers, who contributed to its improvement.

Appendix A. Supplementary data

Supplementary data to this article can be found online at https://doi.org/10.1016/j.palaeo.2022.110961.

References

Agnini, C., Monechi, S., Raffi, I., 2017. Calcareous nannofossil biostratigraphy: historical background and alication in Cenozoic chronostratigraphy. Lethaia 50 (3), 447–463.
Albarède, F., Michard, A., 1987. Evidence for slowly changing $^{87}Sr/^{86}Sr$ in runoff from freshwater limestones of southern France. Chem. Geol. 64, 55–65.
Amadori, C., Garcia-Castellanos, D., Toscani, G., Sternai, P., Fantoni, R., Ghielmi, M., Di Giulio, A., 2018. Restored topography of the Po Plain-Northern Adriatic region during the Messinian base level drop—Implications for the physiography and compartmentalization of the palaeo-Mediterranean basin. Basin Res. 30 (6), 1247–1263.
Andreetto, F., Aloisi, G., Raad, F., Heida, H., Flecker, R., Agiadi, K., Lofi, J., Blondel, S., Bulian, F., Camerlenghi, A., Caruso, A., Ebner, R., Garcia-Castellanos, D., Gaullier, V., Guibourdenche, L., Gvirtzman, Z., Hoyle, T.M., Meijer, P.T., Moneron, J., Sierro, F.J., Travan, G., Tzevahirtzian, A., Vasiliev, I., Krijgsman, W., 2021a. Freshening of the Mediterranean Salt Giant: controversies and certainties around the terminal (Upper Gypsum and Lago-Mare) phases of the Messinian salinity crisis. Earth Sc. Rev. 216, 1–47. https://doi.org/10.1016/j.earscirev.2021.103577.
Andreetto, F., Matsubara, K., Beets, C.J., Fortuin, A.R., Flecker, R., Krijgsman, W., 2021b. High mediterranean water-level during the lago-mare phase of the messinian salinity crisis: insights from the Sr isotope records of Spanish marginal basins (SE Spain). Paleogeogr. Paleoclimatol. Paleoecol. 562.
Angelone, C., Colombero, S., Esu, D., Giuntelli, P., Marcolini, F., Pavia, M., Trenkwalder, S., Van den Hoek Ostende, L.W., Zunino, M., Pavia, G., 2011. Moncucco Torinese, a new post-evaporitic Messinian fossiliferous site from Piedmont (NW Italy). Neues Jahrbuch für Geologie und Paläontologie-Abhandlungen 259, 89–104.
Auer, G., Piller, W.E., Mathias Harzhauser, M., 2014. High-resolution calcareous nannoplankton palaeoecology as a proxy for small-scale environmental changes in the Early Miocene. Mar. Micropaleontol. 111, 53–65. https://doi.org/10.1016/j.marmicro.2014.06.005.
Backman, J., Raffi, I., Rio, D., Fornaciari, E., Pälike, H., 2012. Biozonation and biochronology of Miocene through Pleistocene calcareous nannofossils from low and middle latitudes. Newsl. Stratigr. 45, 221–244.
Baddouh, M.B., Meyers, S.R., Carroll, A.R., Beard, B.L., Johnson, C.M., 2016. Lacustrine $^{87}Sr/^{86}Sr$ as a tracer to reconstruct Milankovitch forcing of the Eocene hydrologic cycle. Earth Planet. Sci. Lett. 448, 62–68. https://doi.org/10.1016/j.epsl.2016.05.007.
Bassetti, M.A., Miculan, P., Sierro, F.J., 2006. Evolution of depositional environments after the end of Messinian Salinity Crisis in Nijar basin (SE Betic Cordillera). Sediment. Geol. 188-189, 279–295.
Beltrando, M., Compagnoni, R., Lombardo, B., 2010. (Ultra-) High-pressure metamorphism and orogenesis: an Alpine perspective. Gondwana Res. 18 (1), 147–166.
Benito, M.I., Suarez-Gonzalez, P., Quijada, I.E., Campos-Soto, S., Rodriguez-Martinez, M., 2021. Constraints of applying strontium isotope stratigraphy in coastal and shallow marine environments: insights from Lower Cretaceous carbonates deposited in an active tectonic setting (N Iberian Basin, Spain). J. Iber. Geol. 47 (1), 151–169.
Bennett, C.E., Williams, M., Leng, M.J., Siveter, D.J., Davies, S.J., Sloane, H.J., Wilkinson, I.P., 2011. Diagenesis of fossil ostracods: Implications for stable isotope based palaeoenvironmental reconstruction. Palaeogeogr. Palaeoclimatol. Palaeoecol. 305 (1–4), 150–161.
Benson, R.H., 1978. The paleoecology of the ostracods of DSDP Leg 42A. In: Hsü, K., Montadert, L. (Eds.), Initial Reports of the Deep-Sea Drilling Project 42. U.S. Government Printing Office, Washington, pp. 777–787.
Bertini, A., 2006. The Northern Apennines palynological record as a contribute for the reconstruction of the Messinian paleoenvironments. Sediment. Geol. 188, 235–258.
Boccaletti, M., Ciaranfi, N., Cosentino, D., Deiana, G., Gelati, R., Lentini, F., Massari, F., Moratti, G., Pescatore, T., Ricci Lucchi, F., Tortorici, L., 1990. Palinspastic restoration and paleogeographic reconstruction of the peri-Tyrrhenian area during the Neogene. Palaeogeogr. Palaeoclimatol. Palaeoecol. 77, 41–50.
Bonaduce, G., Sgarrella, F., 1999. Paleoecological interpretation of the latest Messinian sediments from southern Sicily (Italy). Soc. Geol. Ital. Mem. 54, 83–91.

Bown, P.R., Gibbs, S.J., Sheward, R., O'Dea, S.A., Higgins, D., 2014. Searching for cells: the potential of fossil coccospheres in coccolithophore research. J. Nannoplankt. Res. 34, 5–21.

Brass, G.W., 1976. The variation of the marine $^{87}Sr/^{86}Sr$ ratio during Phanerozonic time: interpretation using a flux model. Geochim. Cosmochim. Acta 40 (7), 721–730.

Brenot, A., Cloquet, C., Vigier, N., Carignan, J., France-Lanord, C., 2008. Magnesium isotope systematics of the lithologically varied Moselle river basin, France. Geochim. Cosmochim. Acta 72 (20), 5070–5089.

Bright, J., Cohen, A.S., Starratt, S.W., 2018. Distinguishing brackish lacustrine from brackish marine deposits in the stratigraphic record: a case study from the late Miocene and early Pliocene Bouse Formation, Arizona and California, USA. Earth Sci. Rev. 185, 974–1003.

Bulian, F., Sierro, F.J., Santiago, L., Jiménez-Espejo, F.J., Bassetti, M.A., 2021. Messinian West Alboran Sea record in the proximity of Gibraltar: early signs of Atlantic-Mediterranean gateway restriction. Mar. Geol. 434 https://doi.org/10.1016/j.margeo.2021.106430.

Carnevale, G., Dela Pierre, F., Natalicchio, M., Landini, W., 2018. Fossil marine fishes and the "Lago Mare" event: has the Mediterranean ever transformed into a brackish lake? Newsl. Stratigr. 51, 57–72. https://doi.org/10.1127/nos/2016/0343.

Carrapa, B., Garcia-Castellanos, D., 2005. Western Alpine back-thrusting as subsidence mechanism in the Tertiary Piedmont Basin (western Po Plain, NW Italy). Tectonophysics 406 (3–4), 197–212.

Caruso, A., Blanc-Valleron, M.M., Da Prato, S., Pierre, C., Rouchy, J.M., 2020. The late Messinian "Lago-Mare" event and the Zanclean Reflooding in the Mediterranean Sea: New insights from the Cuevas del Almanzora section (Vera Basin, South-Eastern Spain). Earth Sci. Rev. 200, 102993 https://doi.org/10.1016/j.earscirev.2019.102993.

Castradori, D., 1998. Calcareous nannofossils in the basal Zanclean of the Eastern Mediterranean Sea: remarks on paleoceanography and sapropel formation. In: Robertson, A.H.F., Emeis, K.C., Richter, C., Camerlenghi, A. (Eds.), Proceedings of the Ocean Drilling Program, Scientific Results 160. US Government Printing Office, Washington, pp. 113–123.

Cipollari, P., Cosentino, D., Radeff, G., Schildgen, T.F., Faranda, C., Grossi, F., Gliozzi, E., Smedile, A., Gennari, R., Darbas, G., Dudas, F.Ö., Gürbüz, K., Nazik, A., Echtler, H., 2013. Easternmost Mediterranean evidence of the Zanclean flooding event and subsequent surface uplift: Adana Basin, southern Turkey. Geol. Soc. Lond., Spec. Publ. 372 (1), 473–494. https://doi.org/10.1144/SP372.5.

Cita, M.B., Wright, R.C., Ryan, W.B.F., Longinelli, A., 1978. Messinian paleoenvironments, in: Hsü, K.J., Montadert, L. et al., Eds.), Initial Reports of the Deep Sea Drilling Project 42. U.S. Government Printing Office, Washington D.C, 1003-1035.

Cita, M.B., Santambrogio, S., Melillo, B., Rogate, F., 1990. Messinian paleoenvironments: new evidence from the Tyrrhenian Sea (ODP LEG 107). In: Proceedings of the Ocean Drilling Program, Scientific Results, 107, pp. 211–227.

Clauzon, G., 1982. Le canyon messinien du Rhöne: Une preuve decisive du "dessicated deep basin model" (Hsü, Cita et Ryan, 1973). Bull. Soc. Geol. Fr. 24, 231–246.

Colombero, S., Bonelli, E., Kotsakis, T., Pavia, G., Pavia, M., Carnevale, G., 2013. Late Messinian rodents from Verduno (Piedmont, NW Italy): biochronological, palaeoecological and palaeobiogeographic implications. Geobios 46, 111–125.

Colombero, S., Angelone, C., Bonelli, E., Carnevale, G., Cavallo, O., Delfino, M., Giuntelli, P., Pavia, G., Pavia, M., Repetto, G., Mazza, P., 2014. The upper Messinian assemblages of fossil vertebrate remains of Verduno (NW Italy): another brick for a latest Miocene bridge across the Mediterranean. Neues Jahrb. Geol. Palaontol. Abh. 272, 287–324.

Colombero, S., Alba, D.M., D'Amico, C., Delfino, M., Esu, D., Giuntelli, P., Harzhauser, M., Mazza, P.P.A., Mosca, M., Neubauer, T.A., Pavia, G., Pavia, M., Villa, A., Carnevale, G., 2017. Late Messinian mollusks and vertebrates from Moncucco Torinese, North-Western Italy. Paleoecological and paleoclimatological implications. Palaeontol. Electron. 20.1.10A, 1–66.

Corbí, H., Soria, J.M., 2016. Late Miocene-early Pliocene planktonic foraminifer event-stratigraphy of the Bajo Segura basin: a complete record of the western Mediterranean. Mar. Pet. Geol. 77, 1010–1027. https://doi.org/10.1016/j.marpetgeo.2016.08.004.

Corbí, H., Soria, J.M., Lancis, C., Giannetti, A., Tent-Manclús, J.E., Dinarès-Turell, J., 2016. Sedimentological and paleoenvironmental scenario before, during, and after the Messinian Salinity Crisis: the San Miguel de Salinas composite section (western Mediterranean). Mar. Geol. 379, 246–266. https://doi.org/10.1016/j.margeo.2016.05.017.

Cosentino, D., Gliozzi, E., Pionzi, G., 2007. The late Messinian Lago-Mare episode in the Mediterranean Basin: preliminary report on the occurrence of Paratethyan ostracod fauna from Central Crete (Greece). Geobios 40 (3), 339–349. https://doi.org/10.1016/j.geobios.2007.01.001.

Cosentino, D., Bertini, A., Cipollari, P., Florindo, F., Gliozzi, E., Grossi, F., Lo Mastro, S., Sprovieri, M., 2012. Orbitally forced paleoenvironmental and paleoclimate changes in the late postevaporitic Messinian of the Central Mediterranean Basin. GSA Bull. 124 (3–4), 499–516. https://doi.org/10.1130/B30462.1.

Cosentino, D., Bracone, V., D'Amico, C., Cipollari, P., Esu, D., Faranda, C., Frezza, V., Gliozzi, E., Grossi, F., Gupperrieri, P., Iadanza, A., Kotsakis, D., Soulié-Märsche, I., 2018. The record of the Messinian salinity crisis in mobile belts: Insights from the Molise allochthonous units (southern Apennines, Italy). Paleogeogr. Paleoclimatol. Paleoecol. 503, 112–130. https://doi.org/10.1016/j.paleo.2018.04.028.

Dal Piaz, G.V., 2010. The Italian Alps: a journey across two centuries of Alpine geology. J. Virtual Explor. 36 (8), 77–106.

De Deckker, P., Lord, A., 2017. Cyprideis torosa: a model organism for the Ostracoda? J. Micropalaeontol. 36 (1), 3–6.

Dela Pierre, F., Clari, P., Cavagna, S., Bicchi, E., 2002. The Parona chaotic complex: a puzzling record of the Messinian (late Miocene) events in Monferrato (NW Italy). Sediment. Geol. 152, 289–311.

Dela Pierre, F., Festa, A., Irace, A., 2007. Interaction of tectonic, sedimentary and diapiric processes in the origin of chaotic sediments: an example from the Messinian of Torino Hill (Tertiary Piedmont Basin, northwestern Italy). Geol. Soc. Am. Bull. 119, 1107–1119.

Dela Pierre, F., Bernardi, E., Cavagna, S., Clari, P., Gennari, R., Irace, A., Lozar, F., Lugli, S., Manzi, V., Natalicchio, M., Roveri, M., Violanti, D., 2011. The record of the Messinian salinity crisis in the Tertiary Piedmont Basin (NW Italy): the Alba section revisited. Palaeogeogr. Palaeoclimatol. Palaeoecol. 310, 238–255.

Dela Pierre, F., Clari, P., Bernardi, E., Natalicchio, M., Costa, M., Cavagna, S., Lozar, F., Lugli, S., Manzi, V., Roveri, M., Violanti, D., 2012. Messinian carbonate-rich beds of the Tertiary Piedmont Basin (NW Italy): microbially-mediated products straddling the onset of the salinity crisis. Palaeogeogr. Palaeoclimatol. Palaeoecol. 34, 78–93. https://doi.org/10.1016/j.palaeo.2012.05.022.

Dela Pierre, F., Clari, P., Natalicchio, M., Ferrando, S., Giustetto, R., Lozar, F., Lugli, S., Manzi, V., Roveri, M., Violanti, D., 2014. Flocculent layers and bacterial mats in the mudstone interbeds of the Primary Lower Gypsum unit (Tertiary Piedmont Basin, NW Italy): archives of paleoenvironmental changes during the Messinian salinity crisis. Mar. Geol. 335, 71–87. https://doi.org/10.1016/j.margeo.2014.05.010.

Dela Pierre, F., Natalicchio, M., Ferrando, S., Giustetto, R., Birgel, D., Carnevale, G., Gier, S., Lozar, F., Marabello, D., Peckmann, J., 2015. Are the large filamentous microfossils preserved in Messinian gypsum colorless sulfide-oxidizing bacteria? Geology 43 (10), 855–858.

Dela Pierre, F., Natalicchio, M., Lozar, F., Bonetto, S., Carnevale, G., Cavagna, S., Clari, P., Colombero, S., Violanti, D., 2016. The Northermost Record of the Messinian Salinity Crisis. Piedmont Basin, NW Italy.

Di Stefano, A., Sturiale, G., 2010. Refinements of calcareous nannofossil biostratigraphy at the Miocene/Pliocene Boundary in the Mediterranean region. Geobios 43 (1), 5–20.

Dimiza, M.D., Koukousioura, O., Michailidis, I., Dimou, V.G., Navrozidou, V., Aligizaki, K., Seferlis, M., 2020. Seasonal living coccolithophore distribution in the enclosed coastal environments of the Thessaloniki Bay (Thermaikos Gulf, NW Aegean Sea). Rev. Micropaleontol. 69, 100449.

Doebbert, A.C., Johnson, C.M., Carroll, A.R., Beard, B.L., Pietras, J.T., Carson, M.R., Norsted, B., Throckmorton, L.A., 2014. Controls on Sr isotopic evolution in lacustrine systems: Eocene green river formation, Wyoming. Chem. Geol. 380, 172–189.

Esu, D., Popov, S.V., 2012. Revision of late Messinian Lymnocardiinae (Bivalvia) from Piedmont (NW Italy). Riv. Ital. Paleontol. Stratigr. 118 (2).

Foeken, J.P.T., Dunai, T.J., Bertotti, G., Andriessen, P.A.M., 2003. Late Miocene to present exhumation in the Ligurian Alps (Southwest Alps) with evidence for accelerated denudation during the Messinian salinity crisis. Geology 31, 707–800.

Fortuin, A.R., Kelling, J.M.D., Roep, T.B., 1995. The enigmatic Messinian -Pliocene section of Cuevas del Almanzora (Vera Basin, SE Spain) revisited-erosional features and strontium isotope ages. Sediment. Geol. 97, 177–201.

Frigui, M., Youssef, M.B., Ouaja, M., 2016. Evidences of "Lago-Mare" episode around the Messinian-Pliocene boundary in eastern Tunisia (Central Mediterranean). J. Afr. Earth Sci. 123, 57–74. https://doi.org/10.1016/j.jafrearsci.2016.07.007.

Gaillardet, J., Dupré, B., Louvat, P., Allegre, C.J., 1999. Global silicate weathering and CO2 consumption rates deduced from the chemistry of large rivers. Chem. Geol. 159 (1–4), 3–30.

Garcia-Castellanos, D., Micallef, A., Estrada, F., Camerlenghi, A., Ercilla, G., Periáñez, R., Abril, J.M., 2020. The Zanclean megaflood of the Mediterranean–Searching for independent evidence. Earth Sci. Rev. 201, 103061.

García-Veigas, J., Cendón, D.I., Gibert, L., Lowenstein, T.K., Artiaga, D., 2018. Geochemical indicators in Western Mediterranean Messinian evaporites: implications for the salinity crisis. Mar. Geol. 403, 197–214. https://doi.org/10.1016/j.margeo.2018.06.005.

García-Veigas, J., Gibert Beotas, L., Cendón, D.I., Dela Pierre, F., Natalicchio, M., Artiaga, D., 2021. Sulfate isotope composition of Messinian evaporites in the Piedmont basin (Italy). Geogaceta 70, 19–22.

Gennari, R., Iaccarino, S.M., Di Stefano, A., Sturiale, G., Cipollari, P., Manzi, V., Roveri, M., Cosentino, D., 2008. The Messinian–Zanclean boundary in the Northern Apennine. Stratigraphy 5, 307–322.

Gennari, R., Lozar, F., Natalicchio, M., Zanella, E., Carnevale, G., Dela, Pierre F., 2020. Chronology of the Messinian events in the northernmost part of the Mediterranean: the Govone section (Piedmont Basin, NW Italy). Riv. Ital. Paleontol. Stratigr. 126, 517–560.

Ghielmi, M., Rogledi, S., Vigna, B., Violanti, D., 2019. La successione messiniana e pliopleistocenica del Bacino di Savigliano (Settore occidentale del Bacino Terziario Piemontese). Geol. Insubrica 13 (1), 140.

Giunta, S., Negri, A., Maffioli, P., Sangiorgi, F., Capotondi, L., Morigi, C., Principato, M. S., Corselli, C., 2006. Phytoplankton dynamics in the eastern Mediterranean Sea during marine isotopic stage 5e. Palaeogeogr. Palaeoclimatol. Palaeoecol. 235 (1–3), 28–47.

Gliozzi, E., Grossi, F., 2008. Late Messinian lago-mare ostracod paleoecology: a correspondence analysis aroach. Paleogeogr. Paleoclimatol. Paleoecol. 264 (3–4), 288–295. https://doi.org/10.1016/j.paleo.2007.03.055.

Gliozzi, E., Ceci, M.E., Grossi, F., Ligios, S., 2007. Paratethyan ostracod immigrants in Italy during the Late Miocene. Geobios 40 (3), 325–337. https://doi.org/10.1016/j.geobios.2006.10.004.

Goudie, A., 2005. The drainage of Africa since the Cretaceous. Geomorphology 67, 437–456.

Grossi, F., Cosentino, D., Gliozzi, E., 2008. Late Messinian Lago-Mare ostracods and paleoenvironments of the central and eastern Mediterranean Basin. Boll. Soc. Paleontol. Ital. 47 (2), 131–146.
Grossi, F., Gliozzi, E., Anadón, P., Castorina, F., Voltaggio, M., 2015. Is Cyprideis agrigentina Decima a good paleosalinometer for the Messinian Salinity Crisis? Morphometrical and geochemical analyses from the Eraclea Minoa section (Sicily). Paleogeogr. Paleoclimatol. Paleoecol. 419, 75–89. https://doi.org/10.1016/j.palaeo.2014.09.024.
Grothe, A., Sangiorgi, F., Brinkhuis, H., Stoica, M., Krijgsman, W., 2018. Migration of the dinoflagellate Galeacysta etrusca and its implications for the Messinian Salinity Crisis. Newsl. Stratigr. 51 (1), 73–91. https://doi.org/10.1127/nos/2016/0340.
Grothe, A., Andreetto, F., Reichart, G.J., Wolthers, M., Van Baak, C.G., Vasiliev, I., Stoica, M., Sangiorgi, F., Middelburg, J.J., Davies, G.R., Krijgsman, W., 2020. Paratethys pacing of the Messinian Salinity Crisis: low salinity waters contributing to gypsum precipitation? Earth Planet. Sci. Lett. 532, 116029 https://doi.org/10.1016/j.epsl.2019.116029.
Grunert, P., Harzhauser, M., Rosenthal, Y., Carnevale, G., 2016. Estuarine Lago Mare fauna from the Tertiary Piedmont Basin indicates episodic Atlantic/Mediterranean exchange during the final stage of the Mediterranean Salinity Crisis. Paleogeogr. Paleoclimatol. Paleoecol. 457, 70–79. https://doi.org/10.1016/j.paleo.2016.06.005.
Guerra-Merchán, A., Serrano, F., Garcés, M., Gofas, S., Esu, D., Gliozzi, E., Grossi, F., 2010. Messinian Lago-Mare deposits near the strait of Gibraltar (Malaga basin, S Spain). Palaeogeogr. Palaeoclimatol. Palaeoecol. 285 (3–4), 264–276.
Guerra-Merchán, A., Serrano, F., Hlila, R., El Kadiri, K., de Galdeano, C.S., Garcés, M., 2014. Tectono-sedimentary evolution of the peripheral basins of the Alboran Sea in the arc of Gibraltar during the latest Messinian-Pliocene. J. Geodyn. 77, 158–170. https://doi.org/10.1016/j.jog.2013.12.003.
Gvirtzman, Z., Manzi, V., Calvo, R., Gavrieli, I., Gennari, R., Lugli, S., Reghizzi, M., Roveri, M., 2017. Intra-Messinian truncation surface in the Levant Basin explained by subaqueous dissolution. Geology 45, 915–918. https://doi.org/10.1130/G39113.1.
Hajj, F., Poszwa, A., Bouchez, J., Guérold, F., 2017. Radiogenic and "stable" strontium isotopes in provenance studies: a review and first results on archaeological wood from shipwrecks. J. Archaeol. Sci. 86, 24–49. https://doi.org/10.1016/j.jas.2017.09.005.
Hällfors, G., 2004. Checklist of Baltic Sea phytoplankton species (including some heterotrophic protistan groups). Baltic Sea Environ. Proc. 95 (1), 208.
Harzhauser, M., Neubauer, T.A., Georgopoulou, E., Esu, D., D'Amico, C., Pavia, G., Giuntelli, P., Carnevale, G., 2015. Late Messinian continental and Lago-Mare gastropods from the Tertiary Piedmont Basin, NW Italy. Bollettino della Società Paleontologica Italiana 54 (1), 1–53. https://doi.org/10.4435/BSPI.2015.1.
Heida, H., Raad, F., Garcia-Castellanos, D., Jiménez-Munt, I., Maillard, A., Lofi, J., 2021. Flexural-isostatic reconstruction of the Western Mediterranean during the Messinian Salinity Crisis: implications for water level and basin connectivity. Basin Res. 34 (1), 50–80. https://doi.org/10.1111/bre.12610.
Hoyle, T.M., Leroy, S.A.G., López-Merino, L., Richards, K., 2018. Using fluorescence microscopy to discern in situ from reworked palynomorphs in dynamic depositional environments-An example from sediments of the late Miocene to early Pleistocene Caspian Sea. Rev. Palaeobot. Palynol. 256, 32–49. https://doi.org/10.1016/j.revpalbo.2018.05.005.
Hsü, K.J., Ryan, W.B.F., Cita, M., 1973. Late Miocene desiccation of the Mediterranean. Nature 242, 240.
Hsü, K.J., Montadert, L., Bernouilli, D., Cita, M.B., Erikson, A., Garrison, R.G., Kidd, R.B., Mélières, F., Müller, C., Wright, R., 1978. History of the Mediterranean salinity crisis. In: Hsü, K.J., Montadert, L., et al. (Eds.), Initial Reports of the Deep Sea Drilling Project. U.S. Government Printing Office, Washington, DC.
Iaccarino, S., Bossio, A., 1999. Paleoenvironment of uppermost Messinian sequences in the western Mediterranean (Sites 974, 975, and 978). In: Proceedings of the Ocean Drilling Program, Scientific Results, Vol. 161. Ocean Drilling Program, College Station, TX, pp. 529–541.
Iaccarino, S.M., Cita, M.B., Gaboardi, S., Gruppini, G.M., 1999. 15. High-Resolution Biostratigraphy at the Miocene/Pliocene boundary in Holes 974b and 975b, Western Mediterranean. In: Proceedings of the Ocean Drilling Program: Scientific Results, Vol. 161, p. 197.
Irace, A., Dela Pierre, F., Clari, P., 2005. "Normal" and "chaotic" deposits in the Messinian Gessoso-Solfifera Fm. at the North-Eastern border of the Langhe domain (Tertiary Piedmont Basin). Bollettino della Società Geologica Italiana, Special Publication 4, 77–85.
Irace, A., Clemente, P., Natalicchio, M., Ossella, L., Trenkwalder, S., De Luca, D., Mosca, P., Piana, F., Polino, R., Violanti, D., 2009. Geologia e idrostratigrafia profonda della Pianura Padana occidentale (Regione Piemonte).
Joordens, J.C.A., Vonhof, H.B., Feibel, C.S., Lourens, L.J., Dupont-Nivet, G., van der Lubbe, J.H.J.L., Sier, M.J., Davies, G.R., Kroon, D., 2011. An astronomically-tuned climate framework for hominins in the Turkana Basin. Earth Planet. Sci. Lett. 307, 1–8. https://doi.org/10.1016/j.epsl.2011.05.005.
Karakitsios, V., Roveri, M., Lugli, S., Manzi, V., Gennari, R., Antonarakou, A., Triantaphyllou, M., Agiadi, K., Kontakiotis, G., Kafousia, N., de Rafelis, M., 2017. A record of the Messinian salinity crisis in the eastern Ionian tectonically active domain (Greece, eastern Mediterranean). Basin Res. 29, 203–233. https://doi.org/10.1111/bre.12173.
Krijgsman, W., Hilgen, F., Raffi, I., Sierro, F., Wilson, D., 1999a. Chronology, causes and progression of the Messinian salinity crisis. Nature 400, 652–655.
Krijgsman, W., Hilgen, F.J., Marabini, S., Vai, G.B., 1999b. New paleomagnetic and cyclostratigraphic age constraints on the Messinian of the Northern Apennines (Vena del Gesso Basin, Italy). Mem. Soc. Geol. Ital. 54, 25–33.
Krijgsman, W., Stoica, M., Vasiliev, I., Popov, V.V., 2010. Rise and fall of the Paratethys Sea during the Messinian Salinity Crisis. Earth Planet. Sci. Lett. 290 (1–2), 183–191. https://doi.org/10.1016/j.epsl.2009.12.020.
Krijgsman, W., Palcu, D., Andreetto, F., Stoica, M., Mandic, O., 2020. Changing seas in the late Miocene Northern Aegean: a Paratethyan aroach to Mediterranean basin evolution. Earth Sci. Rev. 103386 https://doi.org/10.1016/j.earscirev.2020.103386.
Kuznetsov, A.B., Semikhatov, M.A., Gorokhov, I.M., 2012. The Sr isotope composition of the world ocean, marginal and inland seas: Implications for the Sr isotope stratigraphy. Stratigr. Geol. Correl. 20 (6), 501–515.
Lazarev, S., de Leeuw, A., Stoica, M., Mandic, O., van Baak, C.G.C., Vasiliev, I., Krijgsman, W., 2020. From Khersonian drying to Pontian "flooding": late Miocene stratigraphy and paleoenvironmental evolution of the Dacian Basin (Eastern Paratethys). Glob. Planet. Chang. 103224 https://doi.org/10.1016/j.gloplacha.2020.103224.
Lewis, J., Pike, A.W.G., Coath, C., Evershed, R., 2017. Strontium concentration, radiogenic ($^{87}Sr/^{86}Sr$) and stable ($\delta^{88}Sr$) strontium isotope systematics in a controlled feeding study. Sci. Technol. Archaeol. Res. 3, 53–65.
Lirer, F., Foresi, L.M., Iaccarino, S.M., Salvatorini, G., Turco, E., Cosentino, C., Sierro, F.J., Caruso, A., 2019. Mediterranean Neogene planktonic foraminifer biozonation and biochronology. Earth Sci. Rev. 196, 102869.
Loget, N., Davy, P., Van Den Driessche, J., 2006. Mesoscale fluvial erosion parameters deduced from modelling the Mediterranean Sea-level drop during the Messinian (late Miocene). J. Geophys. Res. 111, F03005.
Lozar, F., Violanti, D., Dela Pierre, F., Bernardi, E., Cavagna, S., Clari, P., Irace, A., Martinetto, E., Trenkwalder, S., 2010. Calcareous nannofossils and foraminifers herald the Messinian salinity crisis: the Pollenzo section (Alba, Cuneo; NW Italy). Geobios 43, 21–32.
Lozar, F., Violanti, D., Bernardi, E., Dela Pierre, F., Natalicchio, M., 2018. Identifying the onset of the Messinian salinity crisis: a reassessment of the biochronostratigraphic tools (Piedmont Basin, NW Italy). Newsl. Stratigr. 51 (1), 11–31.
Lugli, S., Vinicio, M., Marco, R., Charlotte, S.B., 2010. The primary lower Gypsum in the Mediterranean: a new facies interpretation for the first stage of the Messinian salinity crisis. Palaeogeogr. Palaeoclimatol. Palaeoecol. 297 (1), 83–99.
Madof, A.S., Bertoni, C., Lofi, J., 2019. Discovery of vast fluvial deposits provides evidence for drawdown during the late Miocene Messinian salinity crisis. Geology 47 (2), 171–174.
Madof, A.S., Ryan, W.B., Bertoni, C., Laugier, F.J., Zaki, A.S., Baumgardner, S.E., 2022. Time-probabilistic approach to the late Miocene Messinian salinity crisis: Implications for a disconnected Paratethys. Terra Nova. https://doi.org/10.1111/ter.12579.
Manzi, V., Lugli, S., Roveri, M., Schreiber, B.C., 2009. A new facies model for the Upper Gypsum of Sicily (Italy): chronological and paleoenvironmental constraits for the Messinian salinity crisis in the Mediterranean. Sedimentology 56, 1937–1960. https://doi.org/10.1111/j.1365-3091.2009.01063.x.
Manzi, V., Gennari, R., Hilgen, F., Krijgsman, W., Lugli, S., Roveri, M., Sierro, F.J., 2013. Age refinement of the Messinian salinity crisis onset in the Mediterranean. Terra Nova 25 (4), 315–322.
Manzi, V., Lugli, S., Roveri, M., Dela, Pierre F., Gennari, R., Lozar, F., Natalicchio, M., Schreiber, B.C., Taviani, M., Turco, E., 2016. The Messinian salinity crisis in Cyprus: a further step towards a new stratigraphic framework for Eastern Mediterranean. Basin Res. 28, 207–236. https://doi.org/10.1111/bre.12107.
Manzi, V., Roveri, M., Argnani, A., Cowan, D., Lugli, S., 2021. Large-scale mass-transport deposits recording the collapse of an evaporitic platform during the Messinian salinity crisis (Caltanissetta basin, Sicily). Sediment. Geol. 424, 106003.
Marcano, M.C., Frank, T.D., Mukasa, S.B., Lohmann, K.C., Taviani, M., 2015. Diagenetic incorporation of Sr into aragonitic bivalve shells: Implications for chronostratigraphic and palaeoenvironmental interpretations. Deposit. Rec. 1 (1), 38–52.
Marchina, C., Natali, C., Fahnestock, M.F., Pennisi, M., Brycec, J., Bianchini, G., 2018. Strontium isotopic composition of the Po river dissolved load: Insights into rock weathering in Northern Italy. Appl. Geochem. 97, 187–196. https://doi.org/10.1016/j.apgeochem.2018.08.024.
Marzocchi, A., Flecker, R., Van Baak, C.G.C., Lunt, D.J., Krijgsman, W., 2016. Mediterranean outflow pump: an alternative mechanism for the Lago-mare and the end of the Messinian Salinity Crisis. Geology 44, 523–526. https://doi.org/10.1130/G37646.1.
McArthur, J.M., Howarth, R.J., Shields, G.A., 2012. Strontium isotope stratigraphy. In: Gradstein, F.M., Ogg, J.G., Schmitz, M.D., Ogg, G.M. (Eds.), The Geological Time Scale 2012. Elsevier B.V, Oxford, pp. 127–144.
McCulloch, M.T., De Deckker, P., 1989. Sr isotope constraints on the Mediterranean environment at the end of the Messinian salinity crisis. Nature 342, 62–65.
Meisch, C., 2000. Freshwater Ostracoda of Western and Central Europe. Spektrum Aakademischer Verlag, Berlin, pp. 1–522.
Meyer, J., Wrozyna, C., Gross, M., Leis, A., Piller, W.E., 2016. Morphological and geochemical variations of Cyprideis (Ostracoda) from modern waters of the northern Neotropics. Limnology. https://doi.org/10.1007/s10201-016-0504-9 first published online October 6, 2016.
Micallef, A., Camerlenghi, A., Garcia-Castellanos, D., Otero, D.C., Gutscher, M.-A., Barreca, G., Spatola, D., Facchin, L., Geletti, R., Krastel, S., Gross, F., Urlaub, M., 2018. Evidence of the Zanclean megaflood in the eastern Mediterranean Basin. Sci. Rep. 8, 1078. https://doi.org/10.1038/s41598-018-19446-3.
Mosca, P., Polino, R., Rogledi, S., Rossi, M., 2009. New data for the kinematic interpretation of the Alps–Apennines junction (Northwestern Italy). Int. J. Earth Sci. https://doi.org/10.1007/s00531-009-0428-2.

Myrow, P.M., 1995. Thalassinoides and the enigma of Early Paleozoic open-framework burrow systems. Palaios 58–74.
Natalicchio, M., Dela Pierre, F., Lugli, S., Lowenstein, T.K., Feiner, S.J., Ferrando, S., Manzi, V., Roveri, M., Clari, P., 2014. Did late Miocene (Messinian) gypsum precipitate from evaporated marine brines? Insights from the Piedmont Basin (Italy). Geology 42, 179–182.
Natalicchio, M., Birgel, D., Peckmann, J., Lozar, F., Carnevale, G., Liu, X., Hinrichs, K.-U., Dela Pierre, F., 2017. An archaeal biomarker record of paleoenvironmental change across the onset of the Messinian salinity crisis in the absence of evaporites (Piedmont Basin, Italy). Org. Geochem. 113, 242–253.
Natalicchio, M., Dela Pierre, F., Birgel, D., Brumsack, H., Carnevale, G., Gennari, R., Gier, S., Lozar, F., Pellegrino, L., Sabino, M., Schnetger, B., Peckmann, J., 2019. Paleoenvironmental change in a precession-paced succession across the onset of the Messinian salinity crisis: Insight from element geochemistry and molecular fossils. Palaeogeogr. Palaeoclimatol. Palaeoecol. 518, 45–61.
Natalicchio, M., Pellegrino, L., Clari, P., Pastero, L., Pierre, F.D., 2021. Gypsum lithofacies and stratigraphic architecture of a Messinian marginal basin (Piedmont Basin, NW Italy). Sediment. Geol. 42, 106009.
Neale, J.W., 1988. Ostracods and palaeosalinity reconstruction. In: De Deckker, P., Colin, J.-P., Peypouquet, J.P. (Eds.), Ostracoda in the Earth Science. Elsevier, Amsterdam, pp. 125–155.
Orszag-Sperber, F., Rouchy, J.M., Blanc-Valleron, M.M., 2000. La transition Messinien-Pliocène en Méditerranée orientale (Chypre): la période du Lago-Mare et sa signification. Comptes Rendus de l'Académie des Sci. Series IIA-Earth Planet. Sci. 331 (7), 483–490.
Palmer, M.R., Edmond, J.M., 1992. Controls over the strontium isotope composition of river water. Geochim. Cosmochim. Acta 56 (5), 2099–2111.
Pełechaty, M., Pukacz, A., Apolinarska, K., Pełechata, A., Siepak, M., 2013. The significance of Chara vegetation in the precipitation of lacustrine calcium carbonate. Sedimentology 60 (4), 1017–1035.
Pellegrino, L., Abe, K., Gennari, R., Lozar, F., Pierre, F.D., Natalicchio, M., Mikami, Y., Jordan, R.W., Carnevale, G., 2020. Integrated micropaleontological study of the Messinian diatomaceous deposits of the Monferrato Arc (Piedmont basin, NW Italy): New insights into the paleoceanographic evolution of the northernmost Mediterranean region. Mar. Micropaleontol. 160, 101910.
Pellen, R., Popescu, S.-M., Suc, J.-P., Melinte-Dobrinescu, M.C., Rubino, J.-L., Rabineau, M., Marabini, S., Loget, N., Casero, P., Cavazza, W., Head, M.J., Aslanian, D., 2017. The Apennine foredeep (Italy) during the latest Messinian: Lago Mare reflects competing brackish and marine conditions based on calcareous nannofossils and dinoflagellate cysts. Geobios 50, 237–257. https://doi.org/10.1016/j.geobios.2017.04.004.
Peucker-Ehrenbrink, B., Fiske, G.J., 2019. A continental perspective of the seawater $^{87}Sr/^{86}Sr$ record: a review. Chem. Geol. 510, 140–165. https://doi.org/10.1016/j.chemgeo.2019.01.017.
Pierre, C., Caruso, A., Blanc-Valleron, M.M., Rouchy, J.M., Orzsag-Sperber, F., 2006. Reconstruction of the paleoenvironmental changes around the Miocene-Pliocene boundary along a West-East transect across the Mediterranean. Sediment. Geol. 188, 319–340. https://doi.org/10.1016/j.sedgeo.2006.03.011.
Placzek, C.J., Quade, J., Patchett, P.J., 2011. Isotopic tracers of paleohydrologic change in large lakes of the Bolivian Altiplano. Quat. Res. 75 (1), 231–244.
Popescu, S.M., Melinte, M.C., Suc, J.P., Clauzon, G., Quillévéré, F., Süto-Szentai, M., 2007. Earliest Zanclean age for the Colombacci and uppermost Di Tetto formations of the "latest Messinian" northern Apennines: New paleoenvironmental data from the Maccarone section (Marche Province, Italy). Geobios 40 (3), 359–373. https://doi.org/10.1016/j.geobios.2006.11.005.
Popescu, S.-M., Dalibard, M., Suc, J.-P., Barhoun, N., Melinte-Dobrinescu, M.C., Bassetti, M.A., Deaconu, F., Head, M.J., Gorini, C., Do Couto, D., Rubino, J.-L., Auxietre, J.-L., Floodpage, J., 2015. Lago Mare episodes around the Messinian-Zanclean boundary in the deep southwestern Mediterranean. Mar. Pet. Geol. 66, 55–70. https://doi.org/10.1016/j.marpetgeo.2015.04.002.
Popescu, S.M., Melinte-Dobrinescu, M.C., Suc, J.P., Do Couto, D., 2017. Ceratolithus acutus (= C. armatus), calcareous nannofossil marker of the marine reflooding that terminated the Messinian salinity crisis: comment on "Paratethyan ostracods in the Spanish Lago-Mare: more evidence for interbasinal exchange at high Mediterranean Sea level" by. Paleogeogr., Paleoclimatol., Paleoecol. 441, 854-870. Paleogeogr. Paleoclimatol. Paleoecol. 485, 986–989. https://doi.org/10.1016/j.paleo.2016.07.011.
Popescu, S.M., Cavazza, W., Suc, J.P., Melinte-Dobrinescu, M.C., Barhoun, N., Gorini, C., 2021. Pre-Zanclean end of the Messinian Salinity Crisis: new evidence from Central Mediterranean reference sections. J. Geol. Soc. https://doi.org/10.1144/jgs2020-183.
Popov, S.V., Shcherba, I.G., Ilyina, L.B., Nevesskaya, L.A., Paramonova, N.P., Khondkarian, S.O., Magyar, I., 2006. Late Miocene to Pliocene palaeogeography of the Paratethys and its relation to the Mediterranean. Palaeogeogr. Palaeoclimatol. Palaeoecol. 238 (1–4), 91–106.
Pross, J., Brinkhuis, H., 2005. Organic-walled dinoflagellate cysts as paleoenvironmental indicators in the Paleogene; a synopsis of concepts. Paläontol. Z. 79 (1), 53–59.
Raad, F., Lofi, J., Maillard, A., Tzevahirtzian, A., Caruso, A., 2021. The Messinian Salinity Crisis deposits in the Balearic Promontory: an undeformed analog of the MSC Sicilian basins?? Mar. Pet. Geol. 104777 https://doi.org/10.1016/j.marpetgeo.2020.104777.
Reghizzi, M., Lugli, S., Manzi, V., Rossi, F.P., Roveri, M., 2018. Orbitally forced hydrological balance during the Messinian Salinity Crisis: insights from Strontium Isotopes ($^{87}Sr/^{86}Sr$) in the Vena del Gesso Basin (Northern Apennines, Italy). Paleoceanogr. Paleoclimatol. 33 (7), 716–731. https://doi.org/10.1029/2018PA003395.
Rossi, M., 2017. Outcrop and seismic expression of stratigraphic patterns driven by accommodation and sediment supply turnarounds: Implications on the meaning and variability of unconformities in syn-orogenic basins. Mar. Pet. Geol. 87, 112–127. https://doi.org/10.1016/j.marpetgeo.2017.03.032.
Rouchy, J.M., Orszag-Sperber, F., Blanc-Valleron, M.M., Pierre, C., Rivière, M., Combourieu-Nebout, N., Panayides, I., 2001. Paleoenvironmental changes at the Messinian-Pliocene boundary in the eastern Mediterranean (southern Cyprus basins): significance of the Messinian Lago-Mare. Sediment. Geol. 145 (1–2), 93–117.
Rouchy, J.M., Pierre, C., Et-Touhami, M., Kerzazi, K., Caruso, A., Blanc-Valleron, M.M., 2003. Late Messinian to Early Pliocene paleoenvironmental changes in the Melilla Basin (NE Morocco) and their relation to Mediterranean evolution. Sediment. Geol. 163 (1–2), 1–27.
Rouchy, J.M., Caruso, A., Pierre, C., Blanc-Valleron, M.M., Bassetti, M.A., 2007. The end of the Messinian salinity crisis: evidences from the Chelif Basin (Algeria). Paleogeogr. Paleoclimatol. Paleoecol. 254 (3–4), 386–417. https://doi.org/10.1016/j.paleo.2007.06.015.
Roveri, M., Bassetti, M.A., Ricci Lucchi, F., 2001. The Mediterranean Messinian Salinity Crisis: an Apennine foredeep perspective. Sediment. Geol. 140, 201–214.
Roveri, M., Bertini, A., Cosentino, D., Di Stefano, A., Gennari, R., Gliozzi, E., Grossi, F., Iaccarino, S.M., Lugli, S., Manzi, V., Taviani, M., 2008a. A high-resolution stratigraphic framework for the latest Messinian events in the Mediterranean area. Stratigraphy 5, 323–342.
Roveri, M., Bertini, A., Cipollari, P., Cosentino, D., Di Stefano, A., Florindo, F., Gennari, R., Gliozzi, E., Grossi, F., Iaccarino, S., Lugli, S., Manzi, V., 2008b. "Earliest Zanclean age for the Colombacci and uppermost Di Tetto formations of the «latest Messinian» northern Apennines: New palaeoenvironmental data from the Maccarone section (Marche Province, Italy)" by Popescu et al.(2007) Geobios 40 (359–373). Geobios 41 (5), 669–675.
Roveri, M., Flecker, R., Krijgsman, W., Lofi, J., Lugli, S., Manzi, V., Sierro, F.J., Bertini, A., Camerlenghi, A., De Lange, G., Govers, R., Hilgen, F.J., Hübscher, C., Meijer, P.T., Stoica, M., 2014a. The Messinian Salinity Crisis: past and future of a great challenge for marine sciences. Mar. Geol. 352, 25–58.
Roveri, M., Lugli, S., Manzi, V., Gennari, R., Schreiber, B.C., 2014b. High resolution strontium isotope stratigraphy of the Messinian deep Mediterranean basins: implications for marginal to central basins correlation. Mar. Geol. 349, 113–125. https://doi.org/10.1016/j.margeo.2014.01.002.
Roveri, M., Manzi, V., Bergamasco, A., Falcieri, F., Gennari, R., Lugli, S., 2014c. Dense shelf water cascading and Messinian canyons: a new scenario for the Mediterranean salinity crisis. Am. J. Sci. 314, 751–784. https://doi.org/10.2475/05.2014.03.
Roveri, M., Gennari, R., Persico, D., Rossi, F.P., Lugli, S., Manzi, V., Reghizzi, M., Taviani, M., 2019. A new chronostratigraphic and paleoenvironmental framework for the end of the Messinian salinity crisis in the Sorbas Basin (Betic Cordillera, southern Spain). Geol. J. 54 (3), 1617–1637. https://doi.org/10.1002/gj.3256.
Ryan, W.B.F., 2009. Decoding the Mediterranean salinity crisis. Sedimentology 56 (1), 95–136.
Sabino, M., Schefuß, E., Natalicchio, M., Dela Pierre, F., Birgel, D., Bortels, D., Schnetger, B., Peckmann, J., 2020. Climatic and hydrologic variability in the northern Mediterranean across the onset of the Messinian salinity crisis. Palaeogeogr. Palaeoclimatol. Palaeoecol. 545, 109632.
Sabino, M., Dela Pierre, F., Natalicchio, M., Birgel, D., Gier, S., Peckmann, J., 2021. The response of water column and sedimentary environments to the advent of the Messinian salinity crisis: insights from an onshore deep-water section (Govone, NW Italy). Geol. Mag. 158 (5), 825–841.
Sardella, R., 2008. Remarks on the Messinian carnivores (Mammalia) of Italy. Boll. Soc. Paleontol. Ital. 47 (2), 195–202.
Schildgen, T.F., Cosentino, D., Frijia, G., Castorina, F., Dudas, F.Ö., Iadanza, A., Sampalmieri, G., Cipollari, P., Caruso, A., Bowring, S.A., Strecker, M.R., 2014. Sea level and climate forcing of the Sr isotope composition of late Miocene Mediterranean marine basins. Geochem. Geophys. Geosyst. 15, 2964–2983. https://doi.org/10.1002/2014GC005332.
Schmid, S.M., Kissling, E., 2000. The arc of the Western Alps in the light of geophysical data on deep crustal structure. Tectonics 19, 62–85.
Sciuto, F., Baldanza, A., Temani, R., Privitera, G., 2018. New reports of Paratethyan ostracods affinity from the Mediterranean Basin (Sicily, Italy). Paleontol. Electron. 21 (1), 1. https://doi.org/10.26879/800.
Skejić, S., Arapov, J., Bužančić, M., Ninčević Gladan, Ž., Bakrač, A., Straka, M., Mandić, J., 2021. First evidence of an intensive bloom of the coccolithophore Syracosphaera halldalii in a highly variable estuarine environment (Krka River, Adriatic Sea). Mar. Ecol. 42 (2), e12641.
Spatola, D., del Moral-Erencia, J.D., Micallef, A., Camerlenghi, A., Garcia-Castellanos, D., Gupta, S., Bohorquez, P., Gutscher, M.A., Bertoni, C., 2020. A single-stage megaflood at the termination of the Messinian salinity crisis: geophysical and modelling evidence from the eastern Mediterranean Basin. Mar. Geol. 106337 https://doi.org/10.1016/j.margeo.2020.106337.
Stoica, M., Lazăr, I., Krijgsman, W., Vasiliev, I., Jipa, D., Floroiu, A., 2013. Paleoenvironmental evolution of the East Carpathian foredeep during the late Miocene-early Pliocene (Dacian Basin; Romania). Glob. Planet. Chang. 103, 135–148. https://doi.org/10.1016/j.gloplacha.2012.04.004.
Stoica, M., Krijgsman, W., Fortuin, A., Gliozzi, E., 2016. Paratethyan ostracods in the Spanish Lago-Mare: more evidence for intra-basinal exchange at high Mediterranean Sea level. Palaeogeogr. Palaeoclimatol. Palaeoecol. 441, 854–870.
Sturani, C., 1973. A fossil eel (Anguilla sp.) from the Messinian of Alba (Tertiary Piedmontese Basin). Palaeoenvironmental and palaeogeographic implications. In: Drooger, C.W. (Ed.), Messinian Events in the Mediterranean. K. Ned. Ak. Wetensch, Amsterdam, pp. 243–255.

Sturani, C., 1976. Messinian facies in the Piedmont basin. Mem. Soc. Geol. It. 16, 11–25.
The venice system for the classification of marine waters according to salinity. Limnol. Oceanogr. 3, 1958, 346–347. https://doi.org/10.4319/lo.1958.3.3.0346.
Thomsen, H.A., 2016. Baltic Sea coccolithophores-an overview of insights into their taxonomy and ecology from the last 40 years. J. Nannoplankton Res. 36 (2), 97–119.
Topper, R.P.M., Lugli, S., Manzi, V., Roveri, M., Meijer, P.T., 2014. Precessional control of Sr ratios in marginal basins during the Messinian salinity crisis? Geochem. Geophys. Geosyst. 15-5, 1926–1944. https://doi.org/10.1002/2013GC005192.
Trenkwalder, S., Violanti, D., D'Atri, A., Lozar, F., Dela Pierre, F., Irace, A., 2008. The Miocene/Pliocene boundary and the early pliocene micropalaeontological record: new data from the Tertiary Piedmont Basin (Moncucco quarry, Torino Hill, Northwestern Italy). Boll. Soc. Paleontol. Ital. 47 (2), 87–103.
Van Baak, C.G., Stoica, M., Grothe, A., Aliyeva, E., Krijgsman, W., 2016. Mediterranean-Paratethys connectivity during the Messinian salinity crisis: the Pontian of Azerbaijan. Glob. Planet. Chang. 141, 63–81. https://doi.org/10.1016/j.gloplacha.2016.04.005.
Vasiliev, I., Reichart, G.-J., Davies, G.R., Krijgsman, W., Stoica, M., 2010. Strontium isotope ratios of the Eastern Paratethys during the Miocene/Pliocene transition; Implications for interbasinal connectivity. Earth Planet. Sci. Lett. 292, 123–131. https://doi.org/10.1016/j.epsl.2010.01.027.
Vasiliev, I., Mezger, E.M., Lugli, S., Reichart, G.J., Manzi, V., Roveri, M., 2017. How dry was the Mediterranean during the Messinian salinity crisis? Paleogeogr. Paleoclimatol. Paleoecol. 471, 120–133. https://doi.org/10.1016/j.paleo.2017.01.032.
Vasiliev, I., Stoica, M., Grothe, A., Lazarev, S., Palcu, D.V., Van Baak, C., De Leeuw, A., Sangiorgi, F., Reichart, G.-J., Davies, G.R., Krijgsman, W., 2021. Hydrological Changes in Restricted Basins: Insights from Strontium Isotopes on late Miocene-Pliocene Connectivity of the Eastern Paratethys (Dacian Basin, Romania). Geochem. Geophys. Geosyst. 22, e2020GC009369 https://doi.org/10.1029/2020GC009369.
Violanti, D., Trenkwalder, S., Lozar, F., Gallo, L.M., 2009. Micropalaeontological analyses of the Narzole core: biostratigraphy and palaeoenvironment of the late Messinian and early Zanclean of Piedmont (Northwestern Italy). Boll. Soc. Paleontol. Ital. 48, 167–181.
Violanti, D., Dela Pierre, F., Trenkwalder, S., Lozar, F., Clari, P., Irace, A., D'Atri, A., 2011. Biostratigraphic and palaeoenvironmental analyses of the Messinian/Zanclean boundary and Zanclean succession in the Moncucco quarry (Piedmont, northwestern Italy). Bull. Soc. géol. France 182 (2), 149–162.
Violanti, D., Lozar, F., Dela Pierre, F., Natalicchio, M., Bernardi, E., Clari, P., Cavagna, S., 2013. Stress tolerant microfossils of a Messinian succession from the northern Mediterranean basin (Pollenzo section, Piedmont, Northwestern Italy). Boll. Soc. Paleontol. Ital. 52, 45–54.
Wade, B.S., Bown, P.R., 2006. Calcareous nannofossils in extreme environment: the Messinian Salinity Crisis, Polemi Basin, Cyprus. Palaeogeogr. Palaeoclimatol. Palaeoecol. 233, 271–286.
Zevenboom, D., 1995. Dinoflagellate cysts from the Mediterranean Late Oligocene and Miocene. Ph.D. Thesis. University of Utrecht, 221 p., 9 pl.; Cip-Gegevens Koninklijke Bibliotheek, Den Haag, The Netherlands.
Zonneveld, K.A., Marret, F., Versteegh, G.J., Bogus, K., Bonnet, S., Bouimetarhan, I., Young, M., 2013. Atlas of modern dinoflagellate cyst distribution based on 2405 data points. Rev. Palaeobot. Palynol. 191, 1–197.